Effects of Cloud Condensation Nuclei and Ice Nucleating Particles on Precipitation Processes and Supercooled Liquid in Mixed-phase Orographic Clouds

Jiwen Fan[1*], L. Ruby Leung[1], Daniel Rosenfeld[2], Paul J. DeMott[3]

[1] Atmospheric Science & Global Change Division, Pacific Northwest National Laboratory, Richland, WA 99352

[2] Institute of Earth Sciences, The Hebrew University of Jerusalem, Jerusalem, 91904 Israel

[3] Department of Atmospheric Science, Colorado State University, Fort Collins, Co, 80523

- Corresponding author:

  jiwen.fan@pnnl.gov

Abstract

How orographic mixed-phase clouds respond to the change of cloud condensation nuclei (CCN) and ice nucleating particles (INPs) are highly uncertain. The main snow production mechanism in warm and cold mixed-phase orographic clouds (referred to as WMOC and CMOC, respectively, distinguished here as those having cloud tops warmer and colder than -20°C) could be very different. We quantify the CCN and INP impacts on supercooled water content, cloud phases and precipitation for a WMOC and a CMOC case with sensitivity tests using the same CCN and INP concentrations between the WMOC and CMOC. It is found that deposition plays a more important role than riming for forming snow in the CMOC, while the role of riming is dominant in the WMOC case. As expected, adding CCN suppresses precipitation especially in WMOC and low INPs. However, this reverses strongly for CCN of 1000 cm^{-3} and larger. We find a new mechanism through which CCN can invigorate mixed-phase clouds over the Sierra Nevada Mountains and drastically intensify snow precipitation when CCN concentrations are high (1000 cm^{-3} or higher). In this situation, more widespread shallow clouds with greater amount of cloud water form in the Central Valley and foothills west of the mountain range. The increased latent heat release associated with the formation of these clouds strengthens the local transport of moisture to the windward slope, invigorating mixed-phase clouds over the mountains, and thereby producing higher amounts of snow precipitation. Increasing INPs leads to decreased riming and mixed-phase fraction in the CMOC but has the opposite effects in the WMOC under all CCN conditions, as a result of liquid-limited and ice-limited conditions, respectively. However, precipitation in both cases is increased by increasing INPs due to an increase of deposition for the CMOC but enhanced riming and deposition in the WMOC. Increasing INPs dramatically reduces supercooled water content and increases the cloud glaciation temperature, while increasing CCN has the opposite effects with much smaller

45 significance.

46

47 **1. Introduction**

48 Snowpack in the Sierra Nevada Mountains is California's largest source of fresh water.
49 Understanding the factors contributing to snow precipitation over the mountains has important
50 implications to predicting the hydrology and local climate of the western U.S. This has motivated
51 a series of CalWater field campaigns carried out since 2009 to improve understanding of
52 processes influencing precipitation and water supply in California (Ralph et al., 2016). Closely
53 linked to precipitation is the distribution of cloud liquid and ice phases, which may be influenced
54 by supercooled liquid commonly occurring in orographic clouds over the Sierra Nevada
55 Mountains (Rosenfeld et al., 2013). Besides precipitation, cloud radiative forcing and cloud
56 feedback in the climate system are also highly dependent on cloud phases because of the very
57 different radiative effect of liquid and ice particles. Hence understanding the key processes and
58 factors impacting cloud phases is critical, but our lack of understanding and ability to model
59 supercooled liquid and cloud phases is limiting skillful predictions at weather and climate time
60 scales.

61 Many factors such as large-scale dynamics, solar heating, and aerosol particles can
62 impact cloud properties and precipitation over the Sierra Nevada Mountains (Shen et al., 2010;
63 Rosenfeld et al., 2008). Atmospheric rivers (ARs) are one of the primary large-scale dynamical
64 features that bring large amount of water vapor from tropics to the U.S. west coast, and can
65 create extreme rainfall and floods (Bao et al 2006; Ralph et al. 2011; Neiman et al. 2010).
66 Aerosols can modify cloud microphysical processes and potentially alter the location, intensity,
67 and type of precipitation (Tao et al., 2012) by acting as cloud condensation nuclei (CCN) or ice
68 nucleating particles (INPs). In California, anthropogenic aerosols from the densely populated

coastal plains and the Central Valley may be incorporated into the frontal airmass before orographic ascent and influence precipitation in the Sierra Nevada Mountains (Rosenfeld and Givati, 2006). Long-range transported aerosols (mainly dust particles) have also been found to have a potential influence on clouds and precipitation in the winter and spring seasons (Uno et al., 2009; Ault et al., 2011; Creamean et al., 2013).

Aerosol impacts on clouds not only depend on aerosol properties such as number, size and composition, but also dynamics and thermodynamics. Rosenfeld et al. (2014) showed significantly different supercooled water (SCW) and precipitation processes in two contrasting cloud cases with air masses containing maritime and continental aerosols, respectively. Many studies have shown that CCN can reduce warm rain precipitation from orographic clouds by reducing the efficiency of cloud droplets conversion into raindrops (e.g., Lynn et al., 2007; Rosenfeld and Givati, 2006; Jirak and Cotton, 2006) and can reduce snowfall precipitation due to reduced riming efficiency (Lowenthal et al., 2011; Rosenfeld et al., 2008). However, some recent studies show a possibility of increased precipitation by CCN in orographic mixed-phase clouds (Fan et al., 2014; Xiao et al., 2015). Other studies have shown that CCN may not have significant effect on the total precipitation, but rather shift precipitation from the windward to leeward slope; a so-called "spillover effect" (Lynn et al., 2007; Saleeby et al., 2011; 2013). By acting as INPs, aerosols can enhance ice growth processes such as deposition and riming and thereby significantly increase snow precipitation (Fan et al., 2014). Both observational and modeling studies have shown that long-range transported dust and biological particles can enhance orographic precipitation in California by serving as INPs (Ault et al., 2011; Creamean et al., 2013, 2014, 2015; Fan et al., 2014).

Besides precipitation, aerosols may have significant impacts on cloud phase and SCW in

92 the mixed-phase clouds, which directly change cloud radiative forcing and Earth's energy
93 balance. Modeling studies have shown that CCN tend to increase SCW via the processes such as
94 suppressed warm rain and/or reduced riming efficiency (Khain et al., 2009; Ilotoviz et al., 2016;
95 Saleeby et al., 2013). A recent observational study corroborated that increasing CCN decreases
96 the cloud glaciation temperature and thus increases the abundance of the mixed-phase regime
97 (Zipori et al., 2015). With abundant INPs such as dust particles, cloud glaciates at a much
98 warmer temperature (Rosenfeld et al., 2011; Zipori et al., 2015). It is found that commonly
99 occurring supercooled water in the clouds near the coastal regions of the western U.S. is
100 associated with low CCN and limited INP conditions (Rosenfeld et al., 2013). Models generally
101 have difficulties to simulate SCW and cloud phases. For example, recent evaluation of the
102 Community Atmosphere Model version 5 (CAM5) with satellite data showed that the model has
103 insufficient liquid cloud and excessive ice cloud from the mid-latitudes to the polar regions, and
104 liquid deficit bias maximizes over the Southern Ocean where supercooled water is prevalent
105 (Kay et al., 2016). For cloud model simulations with cloud-resolving models, ice nucleation
106 parameterizations often need to be modified in order to produce the mixed-phase clouds in the
107 Arctic region (Fan et al., 2009; Fridlind et al., 2007). Considering many microphysical processes
108 are sensitive to aerosol types (CCN or INP), temperature, and/or supersaturation (e.g., deposition
109 growth), aerosol impacts on cloud phase and SCW can be complicated, depending on cloud
110 dynamics and thermodynamics. Our current understanding of cloud microphysical processes
111 impacting SCW and cloud phase in different meteorological environments is poor. Therefore, it
112 is important to conduct process-level studies to improve our understanding.
113 Fan et al. (2014) conducted a study for two mixed-phase orographic cloud cases with
114 different cloud temperatures and showed different significance of the CCN and INP impacts on

115 precipitation between the two cases with much more significant impacts of INPs. The two cases
116 are February 15-16, 2011 (FEB16), and Mar 1-2, 2011 (MAR02). FEB16 has a cloud top
117 temperature as cold as -32°C while the cloud top temperature of MAR02 is generally warmer
118 than -20°C. The temperature differences at the same altitude between the two cases are about 6-
119 10°C. For these reasons, we will herein refer to them as cold mixed-phase orographic clouds
120 (CMOC) and warm mixed-phase orographic clouds (WMOC), respectively. The main snow-
121 forming mechanism in warm and cold mixed-phase orographic clouds could be very different
122 and lead to different precipitation response to changes of CCN and INPs, which has not been
123 studied so far. Following Fan et al. (2014) this study aims to (1) understand the dominant ice
124 growth processes in these two mixed-phase cloud systems; (2) quantify the response of
125 precipitation to the changes of CCN and INPs over a wide range from extremely low to
126 extremely high concentrations, and (3) examine CCN and INP impacts on SCW and cloud
127 phases. The same WRF model with the spectral-bin microphysics (SBM) as used in Fan et al.
128 (2014) is employed. Ice nucleation is parameterized in dependence on mineral dust/biological
129 particle concentrations on the basis of observational evidence. To provide a better process-level
130 understanding and better realize our science goals, the simulation resolution is further increased
131 to be 1-km and the simulations are driven with the 2-km resolution baseline simulation from Fan
132 et al. (2014).
133

134 **2. Model Description and Simulation Design**

135 **2.1 Model description**

136 As in Fan et al. (2014), simulations are performed using WRF version 3.1.1 developed at
137 the National Center for Atmospheric Research (NCAR) (Skamarock et al., 2008) coupled with a

spectral-bin microphysics (SBM) model (Khain et al., 2009; Fan et al., 2012). The SBM is a fast version of the full SBM described by Khain et al. (2004), in which ice crystal and snow (aggregates) in the full SBM are calculated based on one size distribution with separation at 150 μm. ice crystal and snow are referred to as low-density ice. Graupel and hail in the full SBM are grouped as high-density ice, represented with one size distribution without separation. More details about SBM that we used in this study can be found in Fan et al. (2014).

As discussed in Fan et al. (2014), hereafter referred to as FAN2014, the ice nucleation parameterizations in the SBM used for this study have been modified. A new ice nucleation parameterization of DeMott et al. (2015; cited as DeMott et al., 2013 in FAN2014 before the parameterization was published) was incorporated to SBM to investigate the impacts of dust as INPs. The parameterization connects nucleated ice particle concentration under a certain atmospheric condition with aerosol particle number concentration with diameter larger than 0.5 μm ($n_{a>0.5\mu m}$ in Eq. 2 of DeMott et al., 2015). In FAN2014, the aerosol particles that are connected with the DeMott et al. (2015) parameterization are referred to as "dust/bio" (from single particle mass spectral composition measurements), and are based on observations from the Passive Cavity Aerosol Spectrometer Probe (PCASP) for particles with diameter larger than 0.5 μm from clear-sky aircraft data. Note that the actual INP number concentration in the DeMott et al. (2015) parameterization includes an exponential temperature dependence that acts on aerosol concentration, and that the exponent on aerosol concentration is 1.25, so in this paper we vary the constant $n_{a>0.5\mu m}$ over a range of relevant conditions to investigate the impacts of varied INP concentration. It should also be noted that the parameterization is designed and implemented as immersion freezing, that is, a pre-existing liquid particle (droplet or drop) is consumed for each formed ice crystal determined by the parameterization (at the same time, an ice nucleus is

161 removed from the INP category). An added feature of the implementation is that when
162 immersion freezing occurs, freezing starts from the largest drops first, followed by the smaller
163 ones over the size spectrum of water drops. This implementation yielded the majority of large ice
164 particles as observed by aircraft measurements (FAN2014). Adding deposition/condensation
165 freezing produces a large amount of small ice particles, which is not consistent with observations,
166 so deposition/condensation freezing is not included, as discussed in FAN2014. The assumption
167 that the largest drops freeze first also acknowledges the expectation that the largest droplets
168 should have a higher probability of containing an INP active at a given temperature. For contact
169 freezing, we adopt the implementation of Muhlbauer and Lohmann (2009) for the
170 parameterizations described in Cotton et al. (1986) and Young (1974) to connect with INPs. The
171 contribution from the contact freezing with this parameterization is negligible. As described in
172 FAN2014, dust/bio particle concentration (i.e., IN proxy) is a single prognostic variable separate
173 from CCN. For the simulation of the observed case in FAN2014, dust/bio concentration is
174 initiated with the concentration of clear-sky aerosol particles with diameter larger than 0.5 μm in
175 the dust layer. Over-nucleation is prevented by applying an upper limit of ice particle
176 concentration.

177 **2.2 Design of numerical experiments**

178 In FAN2014, simulations were done for the two nested domains with a horizontal grid-
179 spacing of 10 and 2 km, respectively. To focus on the orographic clouds over the Sierra Nevada
180 Mountains and provide a better process-level understanding, we conduct new simulations using a
181 smaller domain of 300 km × 280 km with a grid-spacing of 1 km (the yellow box in Fig. 1a)
182 nested within the 2-km grid-spacing domain of FAN2014 (the blue box). The domain grid points
183 are 301×281 horizontally with 51 vertical levels. The initial and lateral boundary conditions are

produced from the baseline simulations of the 2-km grid-spacing in FAN2014 that were validated by various observational data. The lateral boundary data are updated every 3-hours. The RRTMG shortwave and longwave radiation schemes are used to account for aerosol-cloud-radiation interactions based on the droplet effective radius calculated by SBM.

CCN in the model are represented by a spectrum with 33 size bins with prognostic CCN number concentration for each bin. As stated above, dust/bio particle number concentration serves as a proxy for INP concentration in this region. For the purpose of this study, we conduct sensitivity tests by varying CCN and INP proxy (i.e., dust/bio particle) concentrations over a wide range from the extremely low to extremely high concentrations as shown in Table 1. The initial CCN concentrations for the sensitivity simulations are set to be 30, 100, 300, 1000, and 3000 cm^{-3} (referred to as CCN30, CCN100, CCN300, CCN1000, and CCN3000 respectively). For each CCN condition, simulations are conducted with the initial dust/bio particle concentration of 0.1, 1, 10, and 100 cm^{-3}, respectively, referred to as IN0.1, IN1, IN10, and IN100. Note that the conversion of cm^{-3} dust/bio to INPs per liter is shown in Fig. 10 of DeMott et al. (2015). We also include a table (Table 2) in this study to clearly show the corresponding INP concentrations under different dust/bio particle concentration at a certain temperature. For example, 0.1 cm^{-3} dust/bio means ~0.02 L^{-1} nucleated ice particles at -20^{o}C and ~0.2 L^{-1} at -25^{o}C. These numbers of INPs are akin to the number concentrations of INPs found in the natural marine boundary layer (DeMott et al., 2016). In contrast, 10 cm^{-3} dust/bio, common within some transported dust layers, means ~5 L^{-1} nucleated ice particles at -20^{o}C and ~50 L^{-1} at -25^{o}C (Table 2). The vertical profiles of CCN and INP proxy concentrations at the initial time are uniform below 6 km since observations do not show significant vertical variations as discussed in FAN2014. Simulations are conducted for both cases, and start at 12:00 pm UTC and run for 12

hours since the majority of the convective orographic clouds occur during this period. Note the observed CCN (dust/bio) concentrations for CMOC and WMOC are around 30 (2) and 120 (4) cm^{-3}, respectively.

As described earlier, the CMOC case on FEB16 has cloud top temperatures of about -32°C, which are about 10 degrees colder than the WMOC case on MAR02, and has higher relative humidity (RH) due to the lower temperature although the water vapor mixing ratio is much smaller (Fig. 1b-1d). The temperatures of cloud bases over the mountain slope are about 0°C for the CMOC and about 6°C for the WMOC. Both cases are under the influence of both atmospheric rivers that provide ample water vapor supply and the long-range transported dust/bio. We note however that the lower-level wind directions in the two cases are different, with prevailing westerly and northwesterly on FEB06, and southerly and southwesterly on MAR02. Therefore, the two mixed-phase cloud cases have contrasting thermodynamics and dynamics.

3. Results

3.1 CMOC – FEB16

3.1.1 Precipitation and microphysical processes

Fig. 2a shows the accumulated surface precipitation averaged over the domain for the CMOC case (FEB16). Increasing INPs generally enhances the domain-averaged precipitation except at extremely high CCN concentration (i.e., 3000 cm^{-3}), as a result of increased snow precipitation (Fig. 2c). The sensitivity to INP concentration gets much smaller when INP proxy aerosol concentrations are 10 cm^{-3} and larger. Under the low INP condition where the liquid regime is dominant, the precipitation is first suppressed as CCN increase up to a polluted

condition of 1000 cm^{-3} (grey arrow). This behavior is similar to the CCN effects on shallow warm clouds. As INPs are further increased and mixed-phase clouds are increased, the decreased trend of precipitation with the increase of CCN is changed to a monotonic increasing trend as shown by the brown arrow in Fig. 2a. The most significant feature of Fig. 2a is the sharp increase of surface precipitation from CCN of 1000 to 3000 cm^{-3}, even at the lowest INP condition. This is inconsistent with our previous understanding for deep mixed-phase clouds that precipitation should be significantly suppressed under the extremely polluted conditions because droplets get too small to growth efficiently and the riming also becomes very inefficient (Fan et al., 2007; Li et al., 2008). From Figs. 2b and 2c showing the liquid and snow mass concentrations near the surface (i.e., at the lowest model level of ~ 40 m above the ground), respectively, we see that (1) snow dominates the precipitation for the CMOC case and the ratio of warm rain to total precipitation is very small; and (2) the dramatically enhanced snow explains the sharp increase of precipitation from CCN of 1000 to 3000 cm^{-3}. Note that increasing CCN enhances snow precipitation under any INP condition (Fig. 2c), and warm rain is totally shut off when CCN are 1000 cm^{-3} or larger for the IN0.1 condition (Fig. 2b) due to the much smaller sizes of droplets.

By looking at the in-cloud microphysical properties as shown in Fig. 3, increasing CCN enhances snow number concentration and mass mixing ratio (N_s and Q_s, respectively). Especially, we see a large increase of snow mass from CCN1000 to CCN3000. Cloud ice number concentration and mass mixing ratio (N_i and Q_i, respectively) is also increased. Note ice and snow are represented with a single size spectrum and a threshold size of 150 μm in radius is used to separate them. As discussed in Section 2, the major ice nucleation is through the immersion freezing of DeMott et al. (2015), and with a specification that the largest droplets freeze first

253 when ice nucleation occurs. Therefore, most of the newly-formed ice particles should be large
254 and fall into the snow bins, and so N_s and Q_s contribute more significantly to ice number and
255 mass increase with the increase of CCN than do N_i and Q_i. As CCN increase, not only cloud
256 droplet number concentration (N_c) is increased, but also cloud mass mixing ratio (Q_c). The large
257 increase of Q_c when CCN are high, which corresponds to the large increase of Q_s, will be
258 scrutinized a little later. The decrease of raindrop number concentration and mass mixing ratio
259 (N_r and Q_r, respectively) is very sharp and warm rain becomes negligible when INP proxy
260 aerosol concentrations are 1 cm^{-3} or larger (Fig. 3).

261 From the process rates of the major microphysical processes shown in Fig. 4, we see that
262 the increase of Q_c with the increase of CCN and the decrease of Q_c with the increase of INPs are
263 well explained by the condensation rate (Fig. 4a), although the changes of evaporation have the
264 same trends as well. As shown in Figs. 4c and 4e, deposition is a more significant process than
265 riming except in the case of very low INPs (IN0.1) in this CMOC. Increasing CCN enhances
266 deposition but only enhances riming when CCN are high. The sharp increase of deposition and
267 riming rates from CCN1000 to CCN3000 explains the sharp increase of snow with a major
268 contribution from deposition. How deposition and riming are enhanced so significantly in this
269 case will be elucidated in Section 3.1.2

270 At very low INP concentrations (IN0.1), the riming rate is similar to the deposition rate in
271 this CMOC (Figs. 4c and 4e). As INPs increase, the contribution of riming is reduced
272 significantly because of the reduction of supercooled droplets resulting from increased ice
273 particles in the mixed-phase zone. Thus, the riming process is liquid-limited in this CMOC. As a
274 result of increased ice particles, deposition is enhanced significantly, and it becomes 3-4 times
275 larger than riming in IN10. In the observed condition (i.e., CCN are between 30-300 cm^{-3} and

276 INP proxies range between 1-10 cm^{-3}), both deposition and riming contribute to the snow growth
277 but deposition is the major player. When INP concentrations are extremely high (IN100), clouds
278 glaciate very fast and liquid droplets that are available for riming are limited, so their
279 contribution is negligible (red line in Fig. 4e).

280 The Wegener–Bergeron–Findeisen (WBF) processes refer to ice depositional growth at
281 the expense of liquid through evaporation in mixed-phase clouds. So the mixed-phase cloud
282 regime where vapor pressure falls between the saturation vapor pressure over water and ice is
283 defined as the WBF regime. As CCN increase, the WBF processes get stronger as shown in Figs.
284 5a and 5b. The ratio of the evaporation through WBF to the total evaporation is larger than 0.92
285 in all simulations (Fig. 5a), meaning that drop evaporation in this CMOC occurs predominantly
286 in the WBF regime. There is generally only 50-70% of deposition occurring in the WBF regime
287 even when INP concentrations are in a range (IN0.1 to IN1) that is typical for this region in
288 winter (Fig. 5b), so a significant portion of deposition occurs outside of the WBF regime, and the
289 portion increases as INPs increase. Therefore, increasing INPs generally reduces the WBF
290 regime because of the reduced liquid due to enhanced depositional growth. In this CMOC, the
291 ratio of riming occurring in the WBF regime to the total riming is small (generally around 0.2-
292 0.4 in Fig. 5c), meaning that riming mainly occurs outside of the WBF regimes under any CCN
293 and INP conditions. The ratio is increased by CCN but generally decreased by INPs as a result of
294 the increase/decrease of liquid regime, respectively (Fig. 5c).

295 We see that all major microphysical processes (condensation/evaporation,
296 deposition/sublimation, and riming) are highly sensitive to INPs, while generally having much
297 lower sensitivity to CCN when CCN are below 1000 cm^{-3}. The sensitivity of all the major
298 microphysical processes to CCN gets much more significant when CCN are 1000 cm^{-3} and larger

299 (Fig. 4), associated with significant changes in dynamics and thermodynamics and will be
300 discussed in detail below.
301
302 **3.1.2 Mechanism of enhanced snow precipitation by highly elevated CCN concentrations**
303 Since the results of significant enhanced precipitation from CCN1000 to CCN3000 are
304 unusual, besides verifying the use of identical initial and boundary meteorological conditions in
305 all the experiments to eliminate simulation differences arising from inadvertent factors, we also
306 conducted sensitivity tests by restoring the ice nucleation mechanisms to the default
307 parameterizations (i.e., Meyers et al., 1992 for condensation/deposition and Bigg (1953) for
308 immersing freezing) in the SBM but this yielded a similar conclusion. So, the significantly
309 increased snow precipitation associated with elevated CCN concentrations is not the result of the
310 particular ice-forming parameterization or the implementation approach of the parameterization.
311 Since the precipitation enhancement begins at 1400 UTC, which is a couple of hours into
312 the simulations, we focus on the time period of 14-1600 UTC and use the simulations of
313 different CCN concentrations for the IN1 case to examine the mechanism. By taking a close look
314 at ice nucleation (using model outputs every 6 min), we find that the total nucleated ice particle
315 number concentration is increased as CCN increase and there is a large jump from CCN1000 to
316 CCN3000 (Fig. 6a). The increase is caused by more cloudy points that have ice nucleation (i.e.,
317 immersion freezing) occurring (Fig. 6b) and the enhanced nucleation rate (i.e., the nucleated ice
318 particles per liter of air volume within a hour) in the lower altitudes (Fig. 6c). Considering that
319 the major ice formation mechanism is immersion freezing in this study, which requires the
320 existence of drops for primary nucleation of ice, it means that there is much more supercooled
321 liquid cloud area/volume available for nucleation in the lower altitudes as CCN increase (Fig. 6e).

As shown in Fig. 6d, the increase of cloud water (Q_c) that is supercooled, since the warmest cloud temperature is below 0°C in this case, is very significant, with a big jump from CCN1000 to CCN3000, corresponding to the large increase of snow precipitation. From CCN1000 to CCN3000, the increase of the supercooled liquid area is especially drastic (Fig. 6e).

What causes the drastic increase of Q_c and a more widespread supercooled liquid cloud regime that is available for ice nucleation? We know that the increased drop surface area with the increased CCN can increase condensation, but it cannot explain such a drastic increase of the condensation rate averaged over the entire domain as shown in Fig. 6f. We find that over the domain the updraft area (i.e., grid points with w >1 m s^{-1}) is increased significantly with CCN with a jump from CCN1000 to CCN3000 as well (Fig. 7a), but the averaged updraft velocity does not change significantly (Fig. 7b), suggesting that much more widespread convection occurs to form more clouds in the domain as CCN increase, especially in CCN3000. From the spatial distribution, we see that the increase of clouds is most prominent around the valley and foothills (i.e., the lower-part of the windward slope of the mountains). The cross sections of cloud water, rain and ice/snow mass mixing ratios at 1400 UTC clearly show that more clouds form over the valley and foothills in CCN3000, while in CCN30 there are fewer clouds over the valley and clouds are shallower over the valley and foothills (Fig. 8a). We see much more invigorated mixed-phase clouds in CCN3000 compared with CCN30. The mixed-phase clouds start from the foothills in CCN3000 (Fig. 8c), while CCN30 does not have the mixed-phase clouds present until the regions above the middle and upper part of the mountain slope. This explains the increased ice nucleation rate in the domain at the lower altitudes as shown in Fig. 6c.

The changes of cloud fields described above must involve dynamic and thermodynamic changes. By examining the differences of dynamic and thermodynamic fields between CCN3000

and CCN30 (Fig. 9), we clearly see that a band of increased water vapor and relative humidity (RH) from the valley/foothills to the mountain at the higher altitudes (Fig. 9a-b). The corresponding temperature is only slightly decreased (Fig. 9c), which should not affect the saturation water pressure and ice nucleation efficiency by much. So, the increased RH is mainly caused by the increased water vapor, and this increase can be up to 8% in RH (e.g., from RH of 70% to 78%). The large increase of Q_v and RH is mainly a result of changed local circulation as shown in Figs. 9d-e: the wind blowing to windward slope (zonal wind) gets stronger from CCN30 to CCN3000 (within ~ 2 km above the ground) over the slope. In the cases of atmospheric rivers, the stronger zonal wind transport means an increase of moisture transport to the mountains.

The changes of winds are only significant at the slope of the mountains and occur only after 2 h of the simulations (Fig. 10a), suggesting that they stem from more latent heat release as a result of more clouds over the valley and foothills (feedbacks of radiation and precipitation take much longer time especially considering the two-hour time is 4- 6 am LST). The clouds at the valley/foothill locations are generally shallow. Many literature studies, including both observations and model simulations, have shown that CCN enhance shallow cloud formation and deepen shallow clouds (e.g., Chen et al. 2015; Yuan et al. 2011; Pincus and Baker 1994; Koren et al. 2014), which can be due to various reasons such as cloud lifetime effect, enhanced turbulent convection by larger entrainment rates as a result of stronger evaporation, and greater latent heat release due to larger drop surface area for stronger condensation. We find that condensation is indeed much enhanced over the valley/foothills from CCN30 to CCN3000 under IN1 (Fig. 9f), which results in much reduced supersaturation with respect to water (supersaturation around the cloud base in CCN30 at 1300 UTC is about 0.28% while only 0.04%

368 in CCN3000). The enhanced condensation as well as the cloud lifetime effect (i.e., conversion of
369 smaller droplets into rain is slow and cloud can be sustained for a longer time) contributes to
370 more shallow clouds at the valley/foothills. The more latent heat resulting from enhanced
371 condensation leads to the change of local circulation, which transports more moisture to the
372 windward slope of the mountain, resulting in more active mixed-phase clouds and snow
373 precipitation through enhanced deposition and riming. In addition, over the mountains more
374 supercooled liquid would be lifted to the higher altitudes in the polluted condition, forming
375 ice/snow more efficiently through immersion freezing at the colder temperature, which
376 contributes to more snow precipitation as well.

377 It should be noted that the mixed-phase clouds over the mountains are the key to the
378 enhanced precipitation by CCN. This is confirmed by sensitivity tests based on the WMOC case
379 where ice-related microphysics is turned-off in CCN30IN1 and CCN3000IN1. We chose the
380 WMOC for this sensitivity test because the similar mechanism is present and the WMOC has
381 less mixed-phase regime compared with CMOC, so the factor would have a more significant role
382 in the CMOC if it plays a role in the WMOC. As shown in Fig. 11a, precipitation is dramatically
383 suppressed from CCN of 30 cm^{-3} to 3000 cm^{-3} (Fig. 11a) and there is almost no precipitation at
384 the valley and windward slope in CCN3000 due to extremely small droplets. However, we still
385 see the change of the local circulation over the slope as a result of enhanced condensation (Fig.
386 11b). Therefore, the presence of ice is a necessary condition for such a large increase of
387 precipitation by CCN. Without ice processes (e.g., under the warm season with warm clouds
388 only), precipitation over the mountains can not form efficiently in such a polluted condition even
389 with the increased moisture. But the added latent heat from condensation of vapor to water is still
390 the main energy source of the invigoration.

In summary, increasing CCN forms more clouds at the valley and foothills (generally shallow) through much enhanced condensation, which induces a local circulation change due to more latent heat release that enhances the zonal transport of moisture, leading to the invigoration of the orographic mixed-phase clouds and drastically increased snow precipitation in this CMOC case. Therefore, aerosol impacts on orographic mixed-phase clouds can be extraordinary in extremely polluted conditions, especially under the influence of atmospheric rivers. Besides the the key role of ice processes for leading to greatly enhanced precipitation, orographic dynamics is another important factor since we do not see such impacts in the sensitivity tests where the terrain height is set to be 600 m for the locations with a terrain height > 600 m (precipitation becomes very small in those sensitivity tests and the increase from CCN30 to CCN3000 is small as well).

The increases of Q_v and RH are the most significant from CCN1000 to CCN3000 due to non-linearity of aerosol-cloud interactions, explaining the large increase of snow precipitation. It is worth noting that in CCN3000, warm rain is completely shut off (left column in Fig. 8b), so much more cloud water can be transported to higher altitudes for more immersion freezing, which further enhances the snow precipitation. This likely contributes to the steep increase in precipitation when CCN reach 3000 cm^{-3}.

3.1.3 Supercooled water content (SCW) and cloud phase

By changing the microphysical process rates, CCN and INP impact the cloud phases and supercooled water content (SCW). Fig. 12 shows that INPs have the most striking impact on SCW. Increasing INPs enhances ice particle formation, and then facilitates the deposition and riming processes in this CMOC as discussed in Section 3.1.1. The enhanced deposition in the

WBF regime, along with riming, leads to a faster conversion of liquid to ice in the mixed-phase and glaciates the clouds faster. Therefore, SCW is substantially reduced as INPs increase (Fig. 12a). For example, in the case of CCN300, a significant amount of liquid mass fraction (0.1) exists at the temperature of -30°C for the IN0.1 case. Such temperature is increased to -20, and -10°C as dust/bio INP proxies are increased to 1 and 10 cm^{-3}, respectively. In the extremely high INP case (INP100), there is nearly no supercooled water. As a result, the fractions of cloud phases are dramatically changed (Fig. 13a). As expected, higher INP concentrations decrease the fractions of liquid and mixed phases as the fraction of ice phase increases. In this CMOC, the cloud phases are most sensitive to INPs at relatively low concentrations. For example, for the IN0.1 to IN1 range that is likely common for this region in winter based on observations in the past field campaigns, the liquid phase fraction is reduced by nearly half and the ice phase fraction is increased by 2 times or larger (Fig. 13a). Note that the effects of INPs on cloud phase and SCW presented in this study may represent the upper limit because ice formation is mainly through immersion freezing that transforms the large liquid particles to ice particles when ice forms.

Compared with the effects of INPs, the magnitudes of CCN effects on SCW and cloud phases are much smaller but still significant (the lines with same color but different line styles in Fig. 12). Moreover, the sign is opposite. Increasing CCN generally increases SCW slightly (Figs. 12a). The impact of CCN on cloud phases is generally small, except when INPs are very low, i.e., IN0.1 (Figure 13a). In this low INP case, increasing CCN increases ice phase fractions and reduces the mixed-phase fraction when CCN are relatively low. This is because liquid clouds are dominant so such clouds are sensitive to the CCN-enhanced ice nucleation as discussed in the section 3.1.2.

437

438 **3.2 WMOC – MAR02**

439 For this warm mixed-phase cloud case, the surface accumulated precipitation is
440 suppressed by increasing CCN when CCN are lower than 1000 cm^{-3} (Fig. 14a), which is
441 different from the case of CMOC where the sign of CCN impact on precipitation depends on INP
442 concentration. This is because the clouds in this WMOC behave similarly as warm clouds due to
443 less efficient ice nucleation at the warm cloud temperatures. When CCN are lower than 1000 cm^{-3},
444 the large decrease of warm rain (Fig. 14b) overpowers the slight changes of snow precipitation
445 (Fig. 14c). Similar to the CMOC case, we see a drastic increase of surface precipitation from
446 CCN1000 to CCN3000, also due to drastic increase of snow precipitation. Increasing INPs
447 enhances surface precipitation in a more significant manner than that in CMOC. In other words,
448 the WMOC is more sensitive to INPs than the CMOC.

449 The in-cloud microphysical properties also show similar results as for the CMOC: the
450 steep increases of the snow mass and cloud water mixing ratios from CCN1000 to CCN3000
451 (Fig. 15). We have done the same investigation as in Section 3.1.1, and found the mechanism
452 causing the increased cloud water and the snow production is similar as that in CMOC, that is,
453 increasing CCN forms more shallow clouds at the large area of valley and foothills, which
454 induces a change of local circulation significantly through more latent heat release, which in turn
455 increases the zonal transport of moisture to the windward slope of the mountains. Additionally,
456 more abundant warm rain is present at the wide valley area in this case when CCN are low (30
457 cm^{-3}) compared with the CMOC. The suppression of warm rain as CCN increase is very
458 significant as shown in Figs. 14b and 15. Over the mountain, this suppression increases Q_c and
459 allows more cloud water to be transported to the higher altitudes along the slope where

460 immersion freezing is able to occur at lower temperatures. Ice multiplication through the Hallet-
461 Mossop parameterization (Hallet and Mossop, 1974) in this WMOC contributes to ice particle
462 concentration by 10-15% when CCN are 30 cm^{-3} and INP proxy aerosol concentrations are 1 cm^{-3}
463 in our model simulation with the fast version of SBM in which ice habits are not considered.
464 Therefore, as more ice particles form from immersion freezing when CCN increase, the ice
465 multiplication processes would further increase ice crystal formation although the contribution is
466 relatively small in the model simulation. Past observation studies suggested that ice
467 multiplication through rime-spintering does occur in the orographic mixed-phase clouds of this
468 region (Marwitz 1987; Rauber 1992). We do not yet have a clear understanding of the
469 importance of this process in contributing to ice formation in reality. After more ice particles
470 form, the subsequent ice depositional and riming growth processes form efficient snow
471 precipitation. The CCN impact on local circulation change is more significant in this case
472 compared with the CMOC, probably due to much more shallow warm clouds in the valley.
473 Different from the CMOC case, riming is a more efficient ice growth process to form
474 snow than deposition in this case except when INP concentrations are extremely high (IN100)
475 where both riming and deposition contribute in a similar magnitude (Fig. 16). In addition, the
476 riming rate is increased as INP concentrations increase, which is opposite to that of CMOC. This
477 is because the WMOC is ice-limited and there are not enough ice particles to collide with liquid
478 particles when INP numbers are low, therefore, increasing INPs boosts ice particles and allows
479 more riming to occur. In contrast, the CMOC case is liquid-limited, so increasing INPs reduces
480 liquid particles available for riming due to ice depositional growth. We also see that
481 condensation and evaporation rates are generally more than 2 times larger in this case compared
482 with CMOC and both rates increase more significantly with CCN concentration in this WMOC.

483 This is related to the dominance of liquid clouds in the WMOC. The more significant increase of
484 condensation by increasing CCN compared with the CMOC is likely a result of the more
485 significant change of the local circulation that is associated with more shallow clouds forming at
486 the valley. Increasing INP number concentrations reduces evaporation simply because of the
487 reduction of liquid due to the increased deposition and riming.

488 Similarly as in the CMOC, increasing CCN enhances the WBF process for this WMOC
489 as more droplet evaporation and ice deposition occur (Figs. 17a and 17b). With the increase of
490 CCN, the domain-mean riming rate is not changed much until CCN of 1000 cm^{-3} (Fig. 16e), but
491 the riming rate in the WBF regime is increased (Fig. 17c), possibly due to larger ice particles
492 resulting from stronger deposition growth in the WBF regime.

493 Similar results regarding the CCN and INP impact on supercoooled water content are
494 obtained in the WMOC case as in the CMOC case: increasing INPs dramatically reduces SCW
495 and increases cloud glaciation temperature, while increasing CCN has the opposite effect with
496 much smaller significance (Fig. 12b). Compared with the CMOC, the effects of INPs on SCW
497 are a little smaller but CCN effects are a little larger. The liquid phase fraction (number fraction
498 of cloudy grid points for which the liquid represents 99% or more of the condensate mass)
499 decreases significantly as INPs increase (Fig. 13b). Correspondingly the fractions of the mixed-
500 phase and ice phase cloud volumes increase due to increased ice nucleation. Similar to the
501 increased riming as INPs increase, the mixed-phase fraction is increased as well in the WMOC,
502 which is opposite to the case for CMOC, as a result of the ice-limited condition in the WMOC
503 versus the liquid-limited condition in the CMOC. Note that INP effects are more significant at
504 higher INP concentrations in this case, while in CMOC the sensitivity decreases as INP increases,
505 suggesting that the optimal INP concentration for the maximum INP impact is higher in warmer

clouds than colder clouds, because ice formation at the warmer cloud temperatures is less efficient. The CCN impacts on cloud phase are more significant in this WMOC compared with those in CMOC. The decreased liquid cloud fraction with the increase of CCN is a consequence of the large increase of ice phase fraction resulting from more active cold-cloud processes, since the total cloud fraction sums up to 1 (Fig. 13b).

4. Conclusions and Discussion

Extending the previous study of Fan et al. (2014), we conducted new simulations at higher resolution and further sensitivity studies based on the same two cases of mixed-phase orographic clouds forming on the Sierra Nevada barrier under the influence of atmospheric rivers during the CalWater 2011 field campaign to quantify the response of precipitation to changes of CCN and INPs and to examine CCN and INP impacts on SCW and cloud phases. The two mixed-phase cloud cases have contrasting thermodynamics and dynamics: FEB16 has cold cloud temperatures and northwesterly wind flow at lower-levels (i.e., CMOC), while MAR02 has about 10 °C warmer cloud temperatures and southerly wind flow (i.e., WMOC).

It is found that, in the CMOC case, deposition contributes more significantly to snow production than riming because deposition process is efficient at the cold cloud temperatures (from -22 to -32 °C) in this case. In the WMOC, riming generally contributes more significantly because the deposition growth process is less efficient at the warmer temperatures (generally warmer than -20 °C in this case), except in the extremely high INP case where both riming and deposition contribute similarly.

We find that increasing INP concentrations enhances snow precipitation on the windward slope of the Sierra Nevada Mountains in both CMOC and WMOC cases. With the increase of

INPs, the increased ice nucleation via immersion freezing enhances snow formation by intensifying depositional growth of ice in the CMOC while both deposition and riming contribute in the WMOC. Increasing INPs reduces riming in the CMOC, because of the liquid-limited condition in which more efficient depositional growth at higher INP number concentrations glaciates clouds and reduces liquid particles available for riming. However, in the ice-limited conditions of WMOC, increasing INPs boosts ice particle concentrations so that more riming can occur in a liquid-rich condition. For the same reason, increasing INPs suppresses the WBF processes due to reduced liquid particles.

The CCN impacts on precipitation are complicated, depending on cloud temperature and concentrations of CCN and INPs. When CCN are lower than 1000 cm^{-3}, boosting CCN concentrations slightly increases snow precipitation, but the total precipitation can be increased or decreased depending on the INP concentrations in the CMOC. In contrast, in the WMOC, increasing CCN suppresses the total precipitation due to the large suppression of warm rain production. We find a drastic increase of snow precipitation by increasing CCN when CCN are high (1000 cm^{-3} or larger), consistently in both CMOC and WMOC, as a result of increased deposition and riming rates. The mechanism by which this occurs is through more shallow clouds that form at the wide valley area and foothills with increasing CCN, which induces a change of local circulation through more latent heat release and increases the zonal transport of moisture to the windward slope of the mountains. This results in much more invigorated mixed-phase clouds with enhanced deposition and riming processes and therefore much more snow precipitation. Additionally, over the mountains, the suppression of warm rain as CCN increase allows more cloud droplets to be transported to the higher altitudes where immersion freezing is able to occur efficiently, contributing to the enhanced snow as well. This effect is most

552 significant when warm rain is completely shut off at CCN of 1000 cm^{-3} and higher. Note that
553 this significant CCN impact on precipitation for CCN of 1000 cm^{-3} or larger was not seen in
554 FAN2014, because the CCN concentrations prescribed in that study are smaller than 1000 cm^{-3}.
555 Another difference is that CCN are set to be uniform and increased uniformly over the model
556 domain in this study, while in FAN2014 only the CCN over the Central Valley and coastal urban
557 area were increased.

558 Increasing INP concentrations dramatically reduces supercooled water content and
559 increases cloud glaciation temperature, while increasing CCN has the opposite effect but with
560 much smaller significance. As expected, the fraction of liquid phase clouds is decreased and the
561 ice phase fraction is increased by increasing INP in both cases. However, we see a decreased
562 fraction of mixed-phase clouds by INP in the CMOC but increased in the WMOC, relating to the
563 liquid-limited condition in the former where increasing ice formation enhances cloud glaciation,
564 while the ice-limited condition in the latter in which more liquid clouds are converted to mixed-
565 phase clouds as INPs increase. Compared with the effects of INPs, the magnitudes of CCN
566 effects on SCW and cloud phases are much smaller and the signs are opposite. Increasing CCN
567 generally enhances SCW in both cases. The relative fractions of cloud phases are not much
568 impacted by CCN in the CMOC, except when INPs are very low (i.e., IN0.1). However, in the
569 WMOC, increasing CCN evidently decreases liquid cloud fraction but increases ice phase
570 fraction. Thus, cloud phases in the WMOC have a large sensitivity to CCN compared with
571 CMOC.

572 This study provides a better understanding of the CCN and INP effects on orographic
573 mixed-phase cloud properties and precipitation. The result that CCN dramatically increase snow
574 precipitation over the mountains when CCN are high (l000 cm^{-3} or larger) as a result of modified

575 cloud properties at the valley and foothills is different from previous modeling studies in the
576 literature such as Lowenthal et al. (2011). Many possible reasons could lead to the differences
577 including different cloud cases and different model parameterizations especially for riming
578 processes. The mechanism for the drastic increase of the snow precipitation on the upwind slope
579 by CCN at the very polluted condition is new, and it suggests a strong impact of the shallow
580 clouds at the valley and foothills on the mixed-phase clouds and precipitation over the mountains.
581 It is worth noting that we do not see such a significantly increased precipitation by CCN in the
582 sensitivity tests without ice-related processes or without topography, suggesting that ice
583 processes in the mixed-phase clouds and orographically-forced dynamics are the key factors for
584 such CCN effects. Lynn et al. (2007) also showed that increasing small aerosol particles led to an
585 increased in-cloud snow mass content as a result of more ice particles formed from droplet
586 freezing due to suppressed warm rain formation and thereby more collisions between those ice
587 particles. But different from our study, the total precipitation on the windward slope in Lynn et al.
588 (2007) was decreased as the snow particles had smaller size with lower fall speeds, and they
589 were advected to the lee-side of the mountain, resulting in more precipitation there. The similar
590 mechanism as Lynn et al. (2007) was presented in Noppel et al. (2010) that showed a shift of
591 precipitation from the Mediterranean sea to the land downwind by increased small aerosols
592 because the delayed warm rain formation fostered the formation of extra ice particles with low
593 settling velocity, which were then advected and enhanced precipitation inland. It should be noted
594 that the primary ice nucleation mechanism implemented in the SBM for this study is based on
595 observations and is totally different from those used in Lynn et al. (2007) and Noppel et al.
596 (2010). This could be the reason leading to the different results of aerosol impact on precipitation
597 over the windward slope in our study.

598 The mechanism leading to the enhanced precipitation over the windward slope by
599 increasing CCN is seen in the two cases with very different cloud temperature, wind direction
600 and RH. However, the efficiency of the mechanism could depend on dynamics (wind speed) and
601 thermodynamics (RH). As examined in Lynn et al. (2007), aerosol impact on orographic
602 precipitation is reduced when RH is very high and increased as wind speed is reduced. Over the
603 region of Sierra Nevada Mountains, CCN of above 1000 cm^{-3} would be an extreme condition.
604 Therefore, this mechanism would not occur usually and the change of precipitation would not be
605 much when CCN are less than 1000 cm^{-3} as shown in Fig. 2a and 14a in the normal conditions
606 over this region. We show a precipitation suppression by CCN in the relatively warm situations,
607 in agreement with the observations of Rosenfeld and Givati (2006). However, for many polluted
608 regions such as China and India where CCN of above 1000 cm^{-3} are quite common, this
609 mechanism may have very important implications for orographic precipitation extremes and
610 water cycles.
611 It should be noted that our results of CCN and INP impacts on precipitation and
612 supercooled water content may represent an upper limit since the major ice nucleation in the
613 simulations is through immersion freezing that converts the largest liquid drops into ice or snow
614 directly when ice nucleation occurs, leading to very efficient conversion of liquid to ice/snow
615 and then strong ice growth processes to form snow.
616 In our study, we do not see significant spillover effect of snowfall (i.e., decrease at the
617 windward slope and increase at the leeside slope by increasing CCN) as found in Lynn et al.
618 (2007) and Saleeby et al. (2011). Precipitation mainly forms on the windward slope of the Sierra
619 Nevada Mountains and the increase of the snow precipitation is more significant on the
620 windward slope than on the lee side in both cases. The different results between our study and

621 Saleeby et al. (2011) could be related to different locations of the clouds over the mountain
622 and/or different mountain topography, or the presence of a low-level barrier jet in the
623 atmospheric river environment that reduces the cross barrier flow.
624
625 **Acknowledgements**
626 This study was supported by the California Energy Commission (CEC) and the Office of Science
627 of the U.S. Department of Energy as part of the Regional and Global Climate Modeling program.
628 PNNL is operated for DOE by Battelle Memorial Institute under Contract DE-AC06-
629 76RLO1830. Paul DeMott additionally acknowledges partial support from the U.S. Department
630 of Energy's Atmospheric System Research, an Office of Science, Office of Biological and
631 Environmental Research program, under Grant No. DE-SC0014354.
632

633 **References**

634 Ault, A. P., Williams, C. R., White, A. B., Neiman, P. J., Creamean, J. M., Gaston, C. J., Ralph,
635 F. M., and Prather, K. A.: Detection of Asian dust in California orographic precipitation, J.
636 Geophys. Res., 116, D16205, doi:10.1029/2010JD015351, 2011.
637 Bao, J.-W., Michelson, S. A., Neiman, P.J., Ralph, F. M., and Wilczak, J. M.: Interpretation of
638 enhanced integrated water vapor bands associated with extratropical cyclones: Their
639 formation and connection to tropical moisture, Mon. Wea. Rev., 134, 1063-1080,
640 doi:10.1175/MWR3123.1, 2006.
641 Cesana, G., and Chepfer, H.: Evaluation of the cloud thermodynamic phase in a climate model
642 using CALIPSO-GOCCP, J. Geophys. Res. Atmos., 118, 7922–7937,
643 doi:10.1002/jgrd.50376, 2013.
644 Chen, Y.-C., Christensen, M. W., Diner, D. J., and Garay, M. J.: Aerosol-cloud interactions in
645 ship tracks using Terra MODIS/MISR: J, Geophys. Res., 120, 2819-2833,
646 doi:10.1002/2014jd022736, 2015.
647 Cotton, W., Tripoli, G., Rauber, R., and Mulvihill, E.: Numerical simulation of the effects of
648 varying ice crystal nucleation rates and aggregation processes on orographic snowfall, J.
649 Climate Appl. Meteor., 25, 1658–1680, 1986.
650 Creamean, J. M., Suski, K. J., Rosenfeld, D., Cazorla, A., DeMott, P. J., Sullivan, R. C., White,
651 A. B., Ralph F. M., Minnis P., Comstock, J. M., Tomlinson, J, M., and Prather, K. A.: Dust
652 and Biological Aerosols from the Sahara and Asia Influence Precipitation in the Western
653 U.S., Science, 339, 1572-1578, DOI: 10.1126/science.1227279, 2013.
654 Creamean, J. M., Lee, C., Hill, T. C., Ault, A. P., DeMott, P. J., White, A. B., Ralph, F. M., and
655 Prather, K. A.: Chemical properties of insoluble precipitation residue particles, J Aerosol Sci,
656 76, 13-27, 2014.
657 Creamean, J. M., Ault, A. P., White, A. B., Neiman, P. J., Ralph, F. M., Minnis, P., and Prather,
658 K. A.: Impact of interannual variations in sources of insoluble aerosol species on orographic
659 precipitation over California's central Sierra Nevada, Atmos Chem Phys, 15, 6535-6548,
660 2015
661 DeMott, P. J., Prenni, A. J., McMeeking, G. R., Tobo, Y., Sullivan, R. C., Petters, M. D.,
662 Niemand M., Möhler, O., and Kreidenweis, S. M.: Integrating laboratory and field data to

quantify the immersion freezing ice nucleation activity of mineral dust particles, *Atmos. Chem. Phys.,* 15, 393–409, 2015.

DeMott, P. J., and coauthors: Sea spray aerosol as a unique source of ice nucleating particles, Proceedings of the National Academy of Sciences of the United States of America, 5797–5803, doi: 10.1073/pnas.1514034112, 2016.

Fan, J., Leung, L. R., DeMott, P. J., Comstock, J. M., Singh, B., Rosenfeld, D., Tomlinson, J. M., White, A., Prather, K., Minnis, P., Ayers, J. A., and Min, Q.: Aerosol Impacts on California Winter Clouds and Precipitation during CalWater 2011: Local Pollution versus Long-Range Transported Dust, Atmos. Chem. Phys., 14, 81-101, 2014.

Fan, J., Leung, L. R., Li, Z., Morrison, H., Chen, H., Zhou, Y., Qian, Y., and Wang, Y.: Aerosol impacts on clouds and precipitation in eastern China: Results from bin and bulk microphysics, J. Geophys. Res., 117, D00K36, doi:10.1029/2011JD016537, 2012.

Fan, J., Ovtchinnikov, M., Comstock, J., McFarlane, S. A., and Khain, A.: Ice Formation in Arctic Mixed-Phase Clouds - Insights from a 3-D Cloud-Resolving Model with Size-Resolved Aerosol and Cloud Microphysics, J. Geophys. Res., 114, D04205, doi:10.1029/2008JD010782, 2009.

Fan, J., Zhang, R., Li, G., and Tao, W.-K.: Effects of aerosols and relative humidity on cumulus clouds, J. Geophys. Res., 112, D14204, doi:10.1029/2006JD008136, 2007.

Fridlind, A. M., Ackerman, A. S., McFarquhar, G., Zhang, G., Poellot, M. R., DeMott, P. J., Prenni, A. J., and Heymsfield, A. J.:, Ice properties of single-layer stratocumulus during the Mixed-Phase Arctic Cloud Experiment: 2. Model results, J. Geophys. Res., 112, D24202, doi:10.1029/2007JD008646, 2007.

Hallett, J., and S. C. Mossop: Production of secondary ice particles during the riming process, Nature, 249(5452), 26-28, 1974.

Ilotoviz E., Khain, A. P., Benmoshe, N., Phillips, V. T. J., and Ryzhkov, A.V.: Effect of Aerosols on Freezing Drops, Hail, and Precipitation in a Midlatitude Storm, Journal of the Atmospheric Sciences, 73(1), 109-144, 2016.

Jirak, I. L., and Cotton, W. R.: Effect of air pollution on precipitation along the Front Range of the Rocky Mountains, J. Appl. Meteor. Climatol., 45, 236–245, 2006.

Kay, J. E., Bourdages, L., Miller, N. B., Morrison, A., Yettella, V., Chepfer, H., and Eaton B., Evaluating and improving cloud phase in the Community Atmosphere Model version 5 using

694 spaceborne lidar observations, J. Geophys. Res. Atmos., 121, doi:10.1002/2015JD024699,
695 2016.
696 Khain, A. P., Pokrovsky, A., Pinsky, M., Seifert, A., and Phillips, V.: Simulation of effects of
697 atmospheric aerosols on deep turbulent convective clouds using a spectral microphysics
698 mixed-phase cumulus cloud model. Part I: Model description and possible applications, J.
699 Atmos. Sci., 61, 2963–2982, 2004.
700 Khain, A., Leung. L. R., Lynn, B., and Ghan, S.: Effects of aerosols on the dynamics and
701 microphysics of squall lines simulated by spectral bin and bulk parameterization schemes, J.
702 Geophys. Res., 114, D22203, doi:10.1029/2009JD011902, 2009.
703 Koren, I., Dagan G., and Altaratz O.: From aerosol-limited to invigoration of warm convective
704 clouds. Science, 344, 1143-1146, doi:10.1126/science.1252595, 2014.
705 Li, G., Wang, Y., and Zhang, R.: Implementation of a two-moment bulk microphysics scheme to
706 the WRF model to investigate aerosol-cloud interaction, J. Geophys. Res., 113, D15211,
707 doi:10.1029/2007JD009361, 2008.
708 Lowenthal, D. H., Borys, R. D., Cotton, W., Saleeby, S., Cohn, S. A., and Brown, W. O. J.: The
709 altitude of snow growth by riming and vapor deposition in mixed□phase orographic clouds,
710 Atmos. Environ., 45(2), 519–522, doi:10.1016/j.atmosenv.2010.09.061, 2011.
711 Lynn, B., Khain, A., Rosenfeld, D., and Woodley, W. L.: Effects of aerosols on precipitation
712 from orographic clouds, J. Geophys. Res., 112, D10225, doi:10.1029/2006JD007537, 2007.
713 Marwitz, J. D., Deep Orographic Storms over the Sierra Nevada. Part II: The Precipitation
714 Processes, J. Atmos. Sci., 44(1), 174–185, 1987.
715 Meyers, M. P., DeMott, P. J., and Cotton, W. R.: New primary ice-nucleation parameterizations
716 in an explicit cloud model, J. Appl. Meteor., 31, 708–721, 1992.
717 Muhlbauer, A., and Lohmann, U.: Sensitivity studies of aerosol cloud interactions in mixed-
718 phase orographic precipitation, J. Atmos. Sci., 66(9), 2517–2538,
719 doi:10.1175/2009JAS3001.1., 2009.
720 Neiman, Paul J., Sukovich, E. M., Ralph, F. M., Hughes, M.: A Seven-Year Wind Profiler–
721 Based Climatology of the Windward Barrier Jet along California's Northern Sierra Nevada.
722 Mon. Wea. Rev., 138, 1206–1233, 2010.
723 Noppel H., A. Pokrovsky, B. Lynn , Khain, A. P., and K.D. Beheng 2010: On precipitation
724 enhancement due to a spatial shift of precipitation caused by introducing small aerosols:

numerical modeling. J. Geophys. Res.. 115, D18212, 17 PP., 2010, doi:10.1029/2009JD012645

Pincus, R., and Baker, M. B.: Effect of Precipitation on the Albedo Susceptibility of Clouds in the Marine Boundary-Layer. Nature, 372, 250-252, doi: 10.1038/372250a0, 1994.

Ralph, F. M., Neiman, P. J., Kiladis, G. N., Weickman, K., and Reynolds, D. W.: A multi-scale observational case study of a Pacific atmospheric river exhibiting tropical-extratropical connections and a mesoscale frontal wave. Mon. Wea. Rev., 139, 1169-1189, doi:10.1175/2010MWR3596.1 , 2011.

Ralph, F. M., Prather, K. A., Cayan, D., Spackman, J. R., DeMott, P., Dettinger, M., Fairall, C., Leung, R., Rosenfeld, D., Rutledge, S., Waliser, D., White, A. B., Cordeira, J., Martin, A., Helly, J., and Intrieri, J.: Calwater Field Studies Designed to Quantify the Roles of Atmospheric Rivers and Aerosols in Modulating Us West Coast Precipitation in a Changing Climate, B Am Meteorol Soc, 97, 1209-1228, 2016.

Rauber, R.: Microphysical Structure and Evolution of a Central Sierra Nevada Orographic Cloud System, J. Appl. Meteor., 32, 3-24, 1992.

Rosenfeld, D., and Givati, A.: Evidence of orographic precipitation suppression by air pollution-induced aerosols in the western United States, J. Appl. Meteorol. Climatol., 45(7), 893–911, doi:10.1175/JAM2380.1., 2006.

Rosenfeld, D., Lohmann, U., Raga, G. B., O'Dowd, C. D., Kulmala, M., Fuzzi, S., Reissell, A., and Andreae, M. O.: Flood or drought: How do aerosols affect precipitation?, Science, 321, 1309 – 1313, doi:10.1126/science.1160606, 2008.

Rosenfeld, D., Yu, X., Liu, G., Xu, X., Zhu, Y., Yue, Z., Dai, J., Dong, Z., Dong, Y., and Peng, Y.: Glaciation temperatures of convective clouds ingesting desert dust, air pollution and smoke from forest fires, Geophys. Res. Lett., 38, L21804, doi:10.1029/2011GL049423, 2011

Rosenfeld, D., Rei, Chemke, DeMott, P., Sullivan, R. C., Rasmussen, R., McDonough, F., Comstock, J., Schmid, B., Tomlinson, J., Jonsson, H., Suski, K., Cazorla, A., and Prather, K., The common occurrence of highly supercooled drizzle and rain near the coastal regions of the western United States, J. Geophys. Res. Atmos., 118, doi:10.1002/jgrd.50529, 2013.

Rosenfeld, D., Chemke, R., Prather, K., Suski, K., Comstock, J. M., Schmid, B., Tomlinson, J., and Jonsson, H.: Polluting of winter convective clouds upon transition from ocean inland over central California: Contrasting case studies, Atmos Res, 135, 112-127, 2014/

Saleeby, S. M., Cotton, W. R., and Fuller, J. D. The Cumulative Impact of Cloud Droplet Nucleating Aerosols on Orographic Snowfall in Colorado, Journal of Applied Meteorology and Climatology, 50(3), 604-625, 2011.

Saleeby, S. M., Cotton, W. R., Lowenthal, and Messina, J.: Aerosol Impacts on the Microphysical Growth Processes of Orographic Snowfall, J. Appl. Meteorol. Climatol., 52, 834–850, 2013.

Shen, X., Wang, Y., Zhang, N., and Li, X.: Precipitation and cloud statistics in the deep tropical convective regime, J. Geophys. Res., 115, D24205, doi:10.1029/2010JD014481, 2010.

Tao, W.-K., Chen, J.-P., Li, Z., Wang, C., and Zhang, C.: Impact of aerosols on convective clouds and precipitation, Rev. Geophys., 50, RG2001, doi:10.1029/2011RG000369, 2012.

Uno, I., Eguchi, K., Yumimoto, K., Takemura, T., Shimizu, A., Uematsu, M., Liu, Z., Wang, Z., Hara, Y., and Sugimoto, N.: Asian dust transported one full circuit around the globe, Nat. Geosci., 2(8), 557–560, doi:10.1038/ngeo583, 2009.

Xiao, H., Yin, Y., Jin, L., Chen, Q., and Chen, J.: Simulation of the effects of aerosol on mixed-phase orographic clouds using the WRF model with a detailed bin microphysics scheme, J. Geophys. Res. Atmos., 120, 8345–8358, doi:10.1002/ 2014JD022988, 2015.

Young, K. C.: A numerical simulation of wintertime, orographic precipitation. Part I: Description of model microphysics and numerical techniques. J. Atmos. Sci., 31,1735–1748, 1974.

Yuan, T., Remer, L. A., and Yu, H.: Microphysical, macrophysical and radiative signatures of volcanic aerosols in trade wind cumulus observed by the A-Train. Atmos. Chem. Phys, 11, 7119-7132, 2011.

Zipori, A., Rosenfeld, D., Tirosh, O., Teutsch, N., and Erel, Y.: Effects of aerosol sources and chemical compositions on cloud drop sizes and glaciation temperatures, J. Geophys. Res. Atmos., 120, 9653–9669, doi:10.1002/2015JD023270, 2015

Table 1 Model simulations that are run for different CCN and INP proxy aerosol concentrations. Please note that INP proxy aerosol concentrations denote dust/bio particle number concentrations with particle size > 0.5 μm for use in the parameterization of DeMott et al. (2015), as described in FAN2014.

		INP proxy aerosol concentrations (cm^{-3})			
		0.1	1	10	100
CCN (cm^{-3})	30	x	x	x	x
	100	x	x	x	x
	300	x	x	x	x
	1000	x	x	x	x
	3000	x	x	x	x

Table 2 INP concentrations (L^{-1}) calcuated based on DeMott et al. (2015) under different INP proxy aerosol concentrations (i.e., dust/bio particles in this study) at the various tempertures.

Dust/bio (cm^{-3})	Temperature (°C)						
	-5	-10	-15	-20	-25	-30	-35
0	0.00	0.00	0.00	0.02	0.15	1.52	15.19
1	0.00	0.00	0.03	0.27	2.71	27.08	270.05
10	0.00	0.05	0.49	4.84	48.27	481.47	4802.27
100	0.09	0.87	8.63	86.06	858.40	8561.88	85397.75

804
805 **Figures**

806

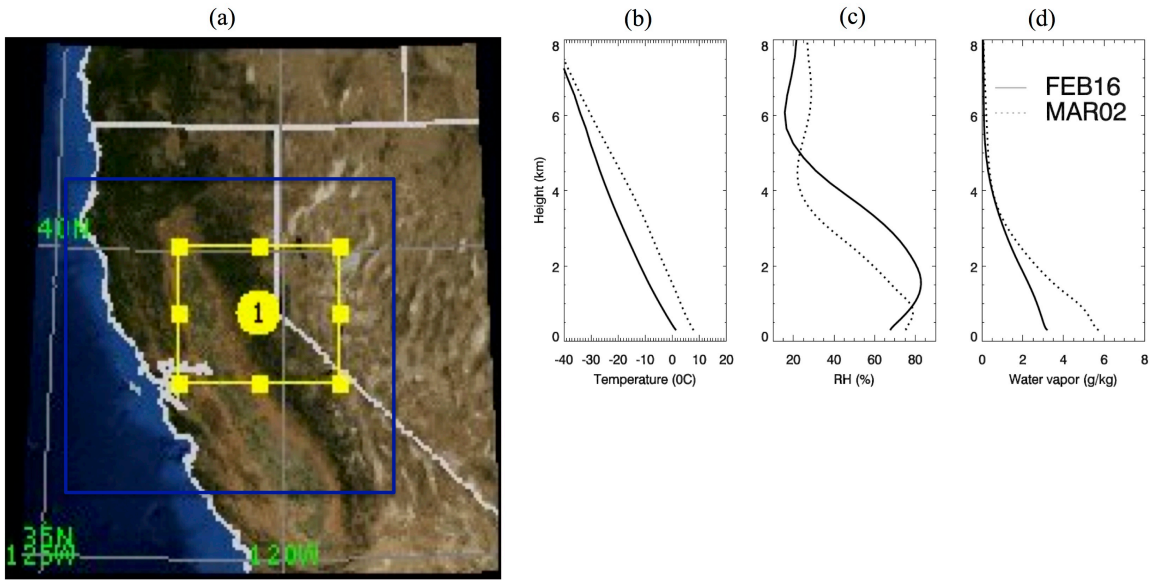

Fig. 1 (a) The simulation domain (yellow box), and the vertical profiles of (b) the temperature, (c) RH, and (d) water vapor for CMOC (FEB16) and WMOC (MAR02). (b)-(d) are domain mean values during the model simulation time period. The blue box in (a) denotes the domain of 2 km resolution simulations done in FAN2014.

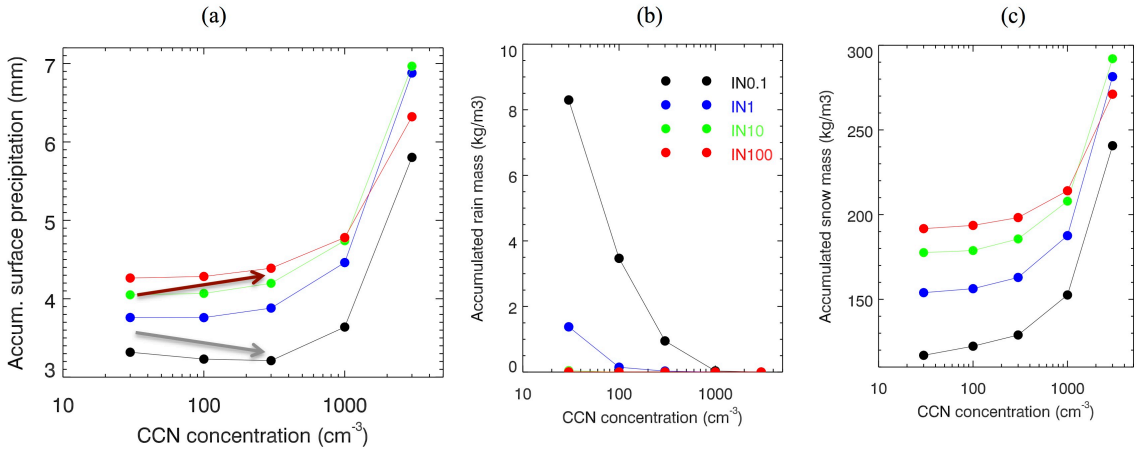

Fig. 2 (a) The domain-mean accumulated surface precipitation, and the accumulated (b) rain and (c) snow mass concentrations at the lowest model level (~ 40 m above the surface) during the simulation time period for CMOC. All domain- mean calculation excludes the lateral boundary grid points in this study. The grey arrow indicates the decrease trend under low INP proxy concentrations and the magenta arrow is for the increase trend under high INP proxy concentrations.

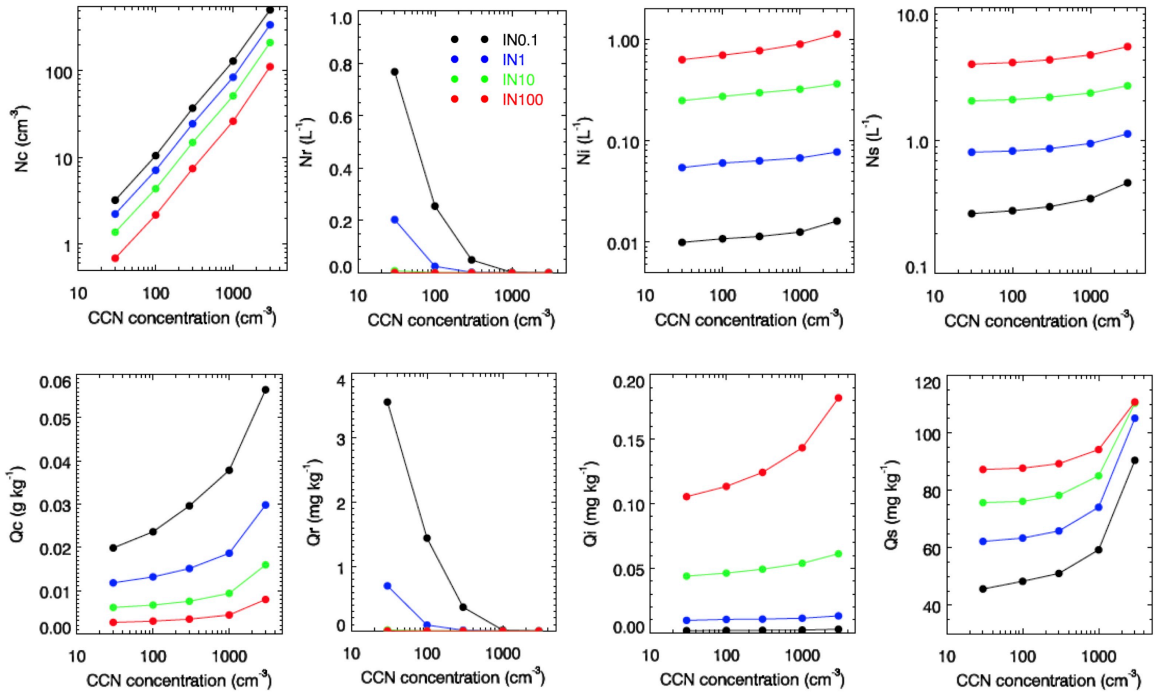

Fig. 3 The number concentrations (top row) and mass mixing ratios (bottom row) of droplet (1st column), rain (2nd column), cloud ice (3nd column), and snow (4th column) for CMOC. The data are averaged over the grid points over the domain by excluding the lateral boundary grid points below the 7 km altitude and over the simulation time by excluding the initial two hours.

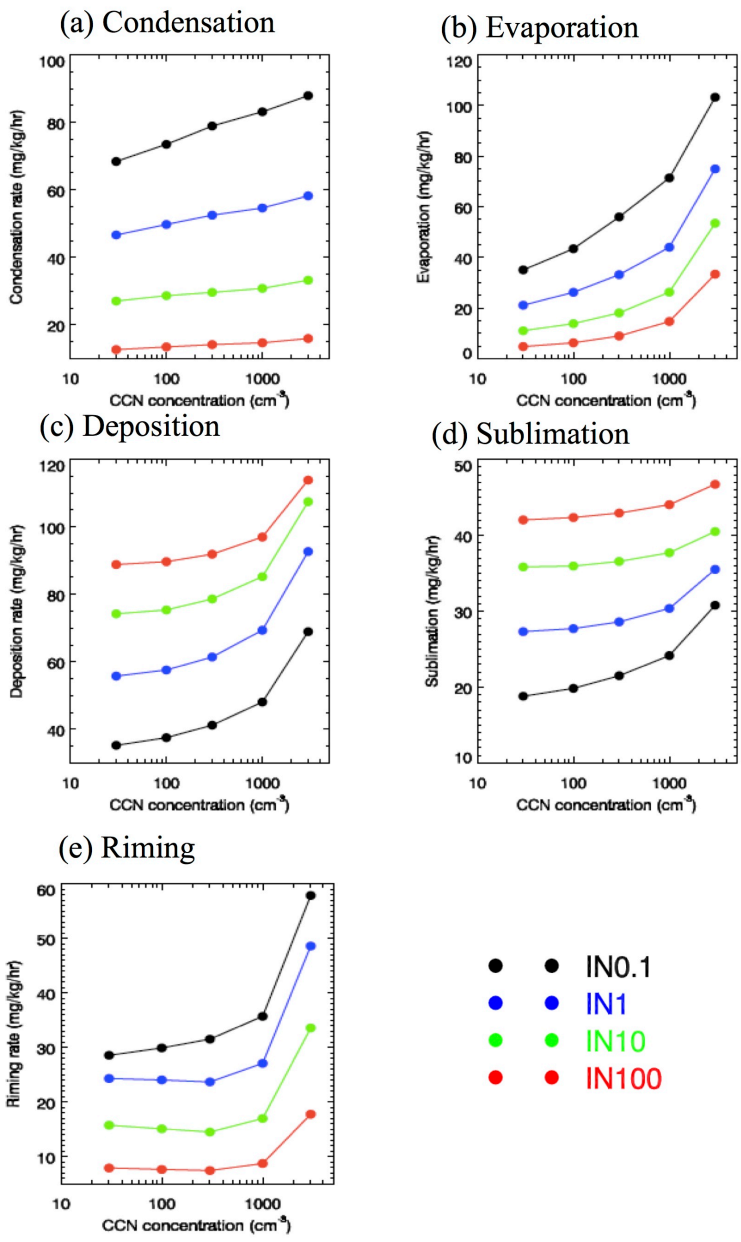

Fig. 4 The microphysical process rates of (a) condensation, (b) evaporation, (c) deposition, (d) sublimation, and (e) riming for CMOC. The model outputs for the process rates are in every 6 min frequency, and the data shown in the plots were processed in the same way as Fig. 3.

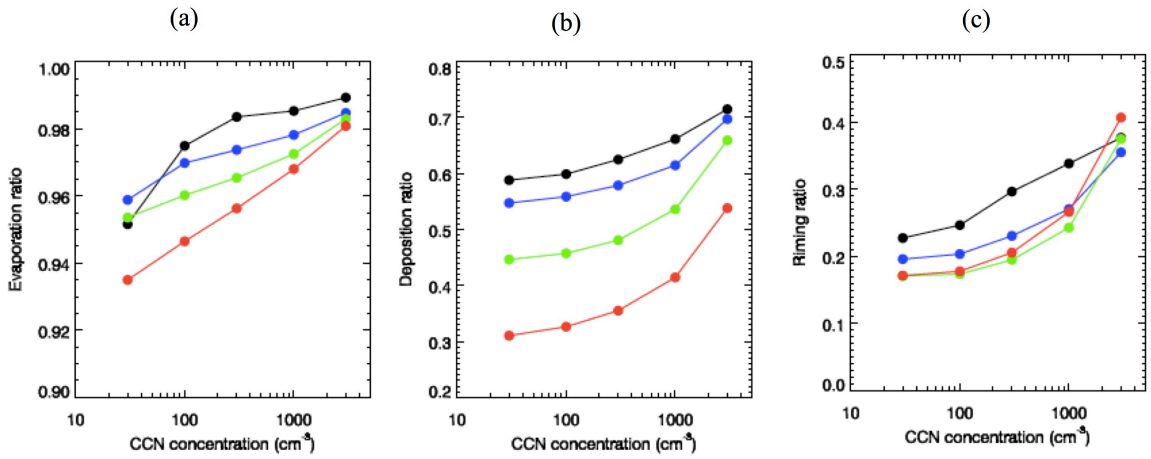

Fig. 5 (a) The ratio of evaporation occurring in the WBF regime that is defined as the grid points where the WBF processes occur) to the total evaporation for the CMOC case. (b) and (c) are the same as (a), except for deposition and riming, respectively. Data were processed in the same way as Fig. 3. Lines and symbols follow Fig. 3.

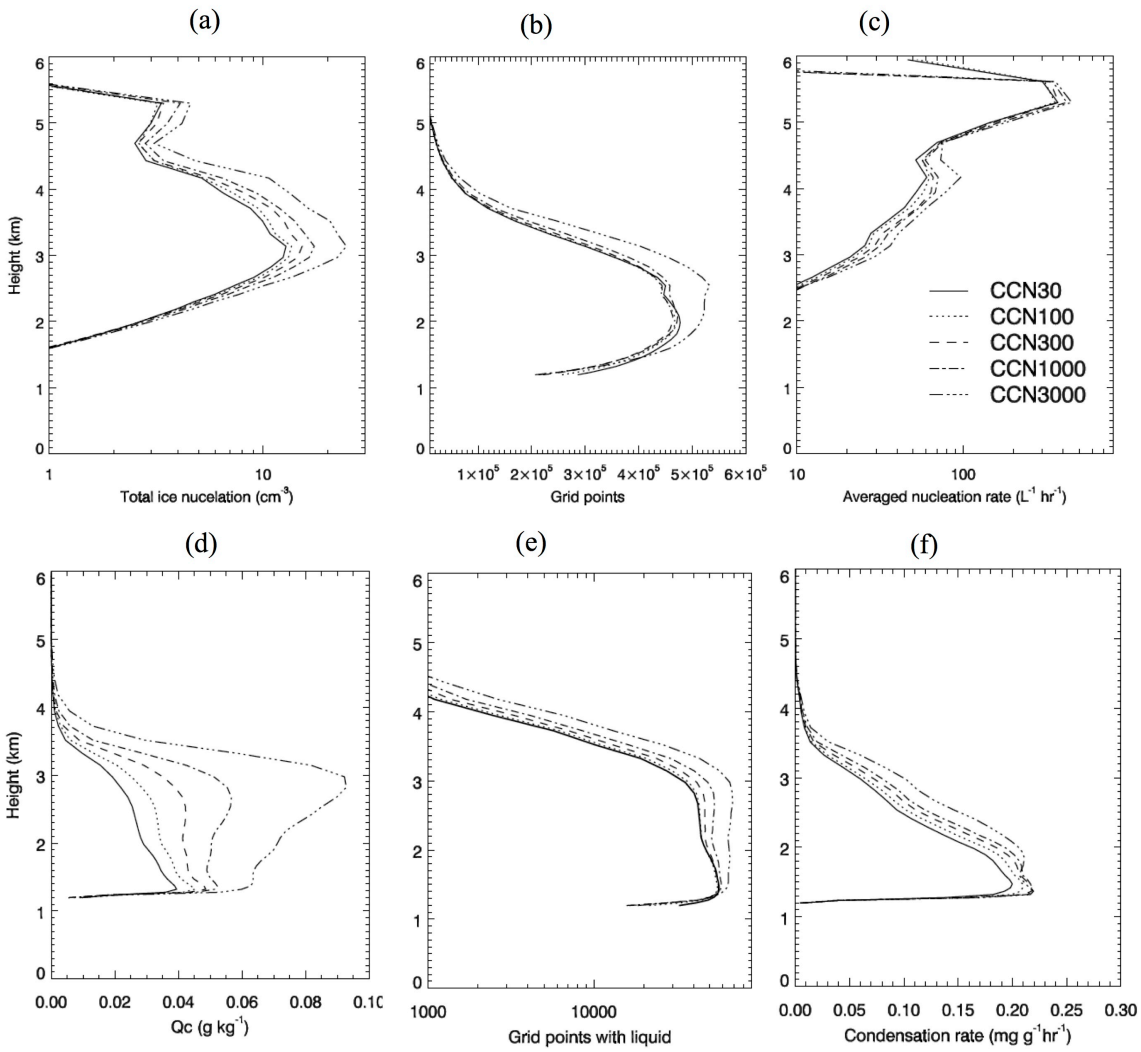

Fig. 6 Vertical profiles of (a) total nucleated ice particles, (b) the total grid points where ice nucleation occurs, (c) the ice nucleation rate averaged over the total ice nucleation grid points, (d) domain-mean cloud water content (Q_c), (e) the total grid points that have liquid (i.e., the liquid water mixing ratio is larger than 1.e-5 kg kg^{-1}), and (f) the domain-mean condensate rate during 1400-1600 UTC for the CMOC case.

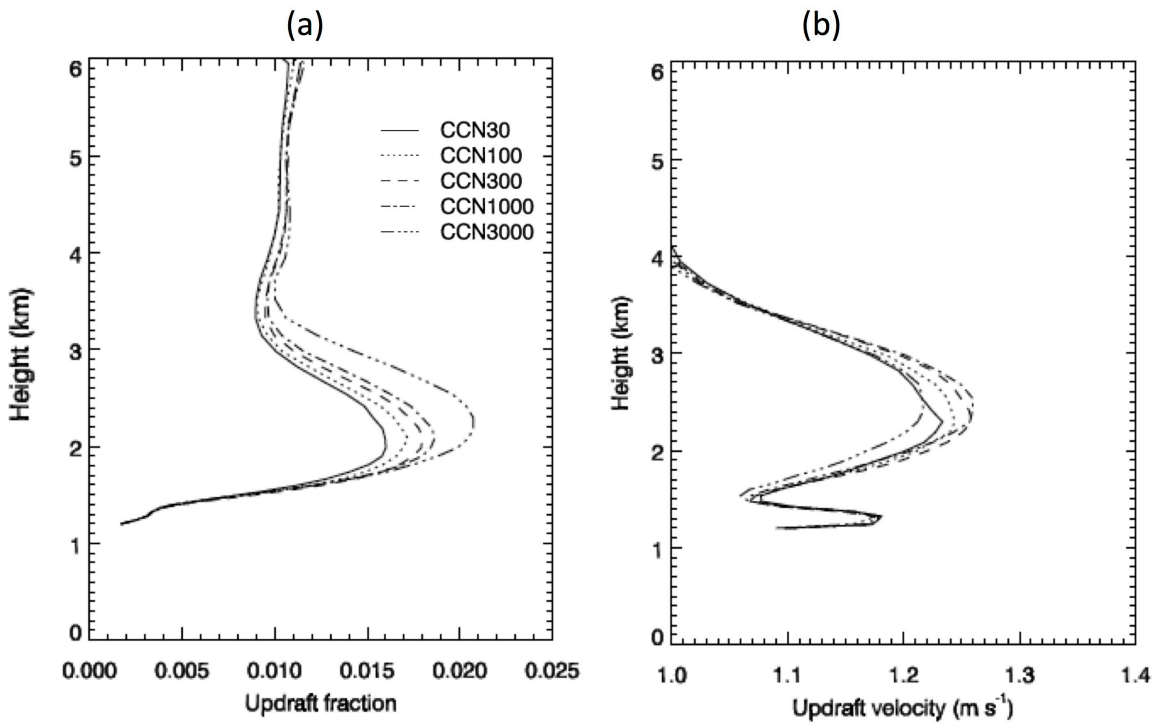

Fig. 7 (a) The fraction of updraft grid points with vertical velocity larger than 1 m s^{-1} relative to the total domain grid points, and (b) the mean updraft velocity for the grid points larger than 1 m s^{-1} over 1400-1600 UTC for the CMOC case.

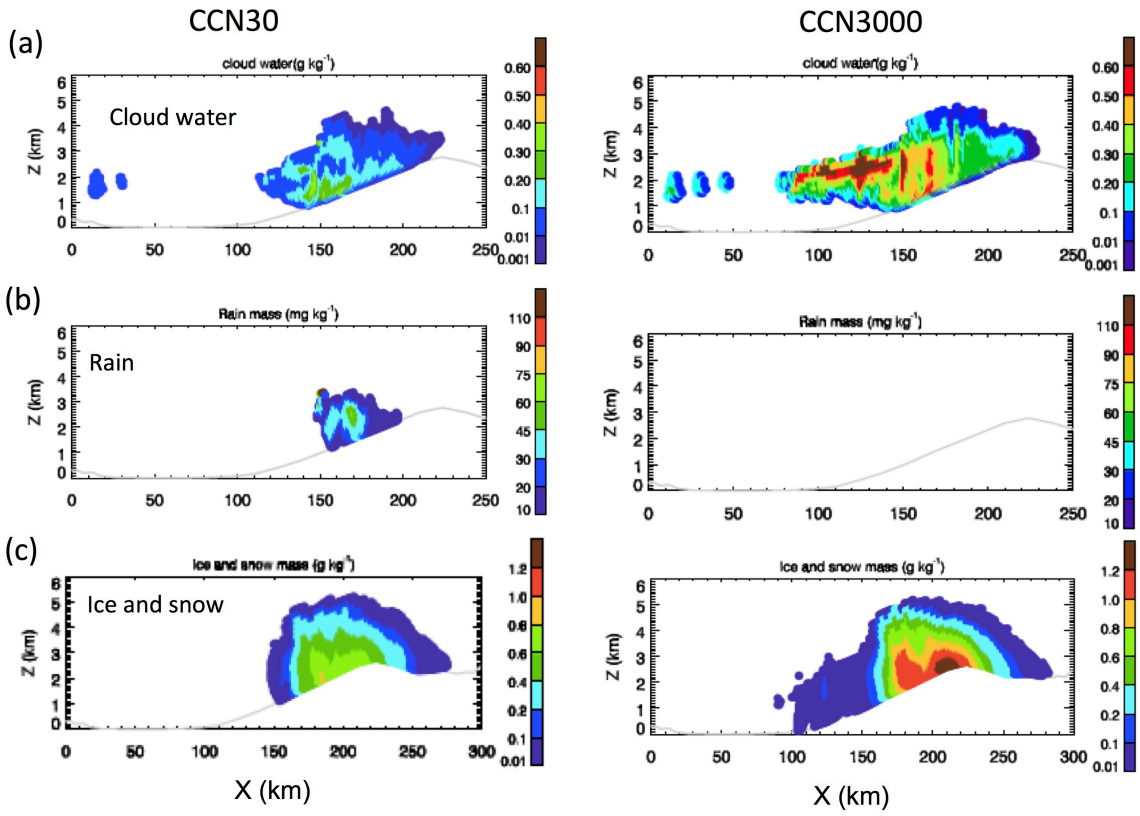

Fig. 8 The west-east cross section of (a) cloud water content, (b) rain water content, and (c) ice and snow water content for CCN30 (left) and CCN3000 (right) with INP proxy concentrations of 1 cm^{-3} at 1400 UTC averaged over the 20 km wide area zonally for the CMOC.

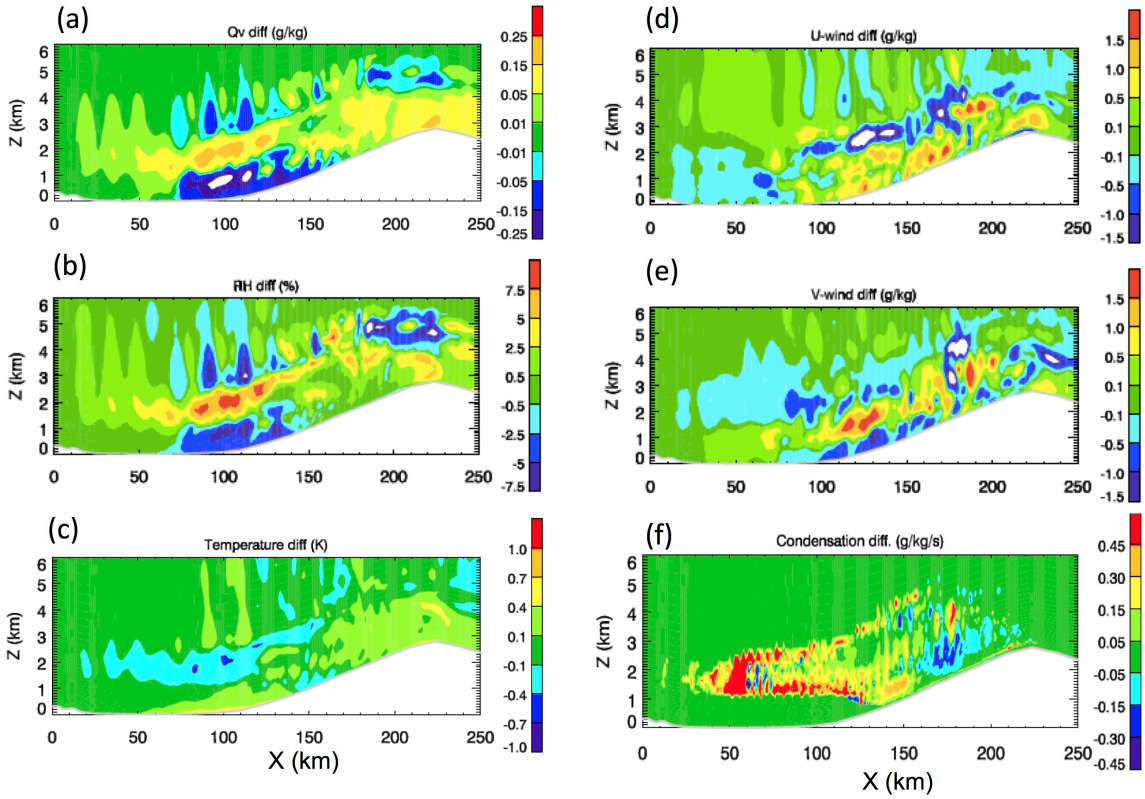

Fig. 9 Differences of (a) water vapor, (b) RH, (c) temperature, (d) U-component of the wind, (f) V- component of the wind, and (f) condensation rate between CCN3000 and CCN30 with INP proxy concentration of 1 cm^{-3} for the CMOC. The cross section area is same as Fig. 8. The time is at 1400 UTC except that the condensation rate used for the difference calculation is the sum of that from 1300-1400 UTC to show an accumulated value over 1-hour period before 1400 UTC.

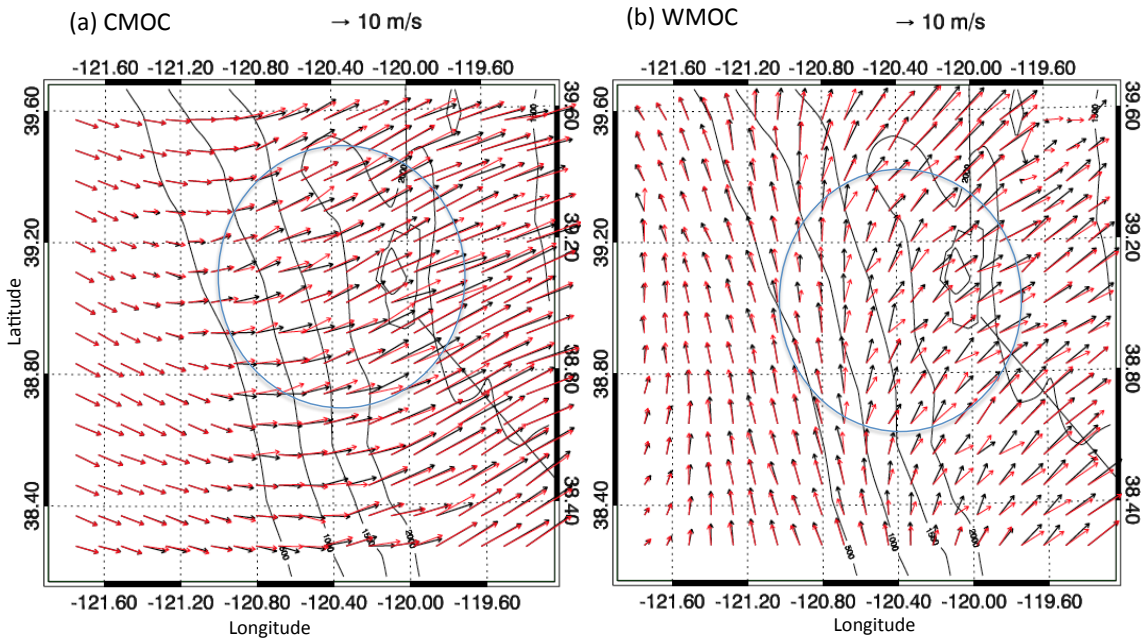

Fig. 10 The spatial distribution of wind field at about 1.7 km above the ground for (a) CMOC and (b) WMOC at 1400 UTC. The red color denotes CCN3000 and black color denotes CCN30 with IN1. The grey contour lines are the geophysical height in meters. The blue cycle is to mark the area with significant changes of wind (i.e., over the wind ward slope of the mountain).

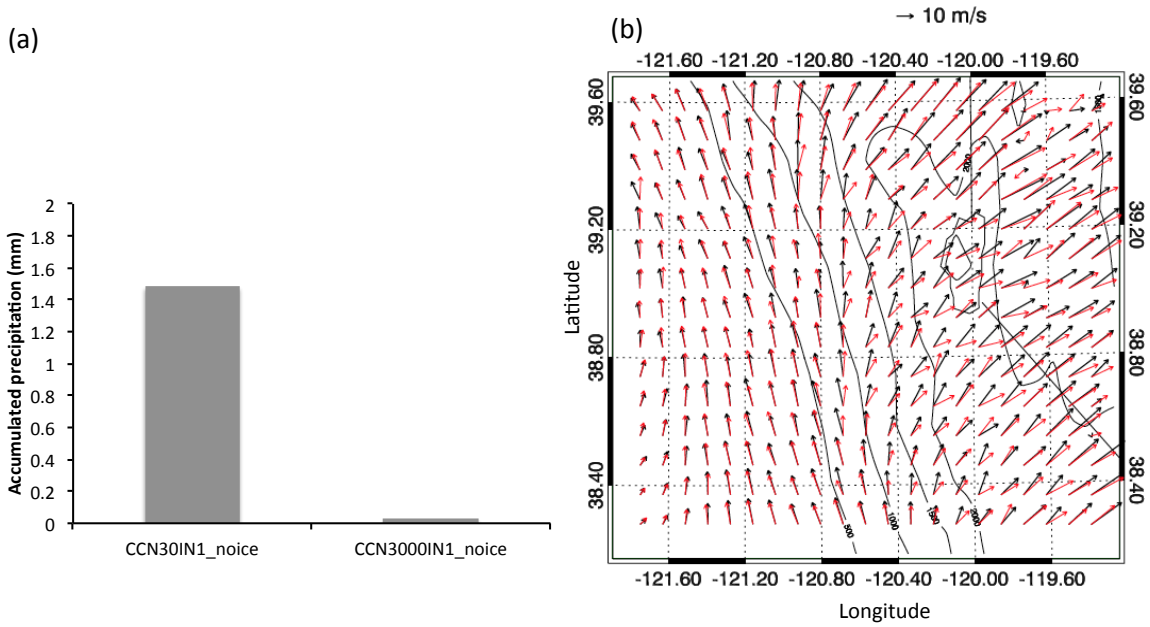

Fig. 11 Results for the two simulations without ice-related microphysics, i.e., CCN30IN1_noice and CCN3000IN1_noice, which are based on CCN30IN1 and CCN3000IN1, respectively, for the WMOC case: (a) the domain averaged accumulated precipitation, and (b) the spatial distribution of wind field at about 1.7 km above the ground at 1400 UTC. The red color on (b) denotes CCN3000IN1_noice and black color denotes CCN30IN1_noice.

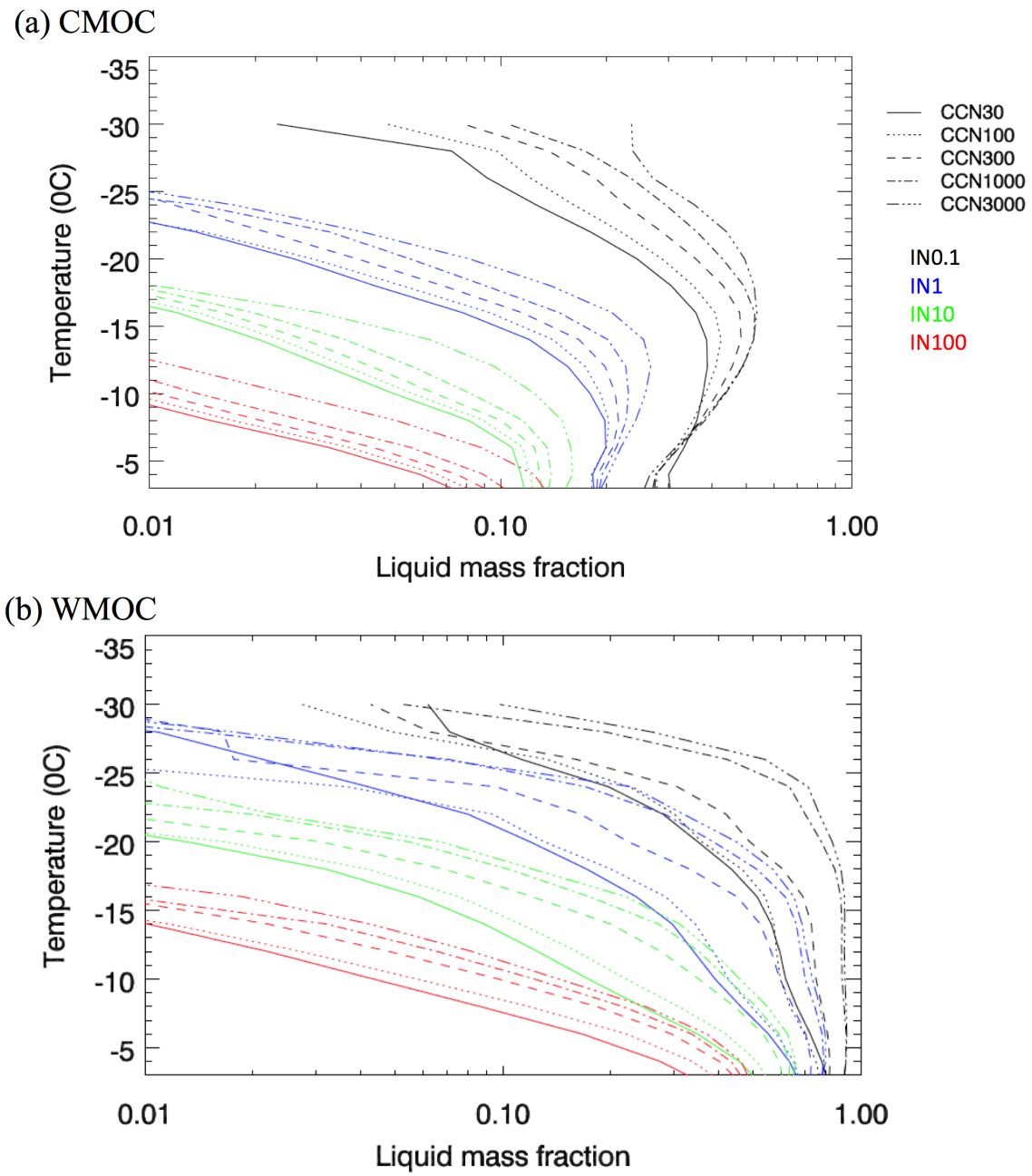

Fig. 12 The liquid mass fraction vs. temperature for the (a) CMOC and (b) WMOC over the simulation time by excluding the initial two hours. The liquid mass fraction is calculated for each temperature bin of a 2 K interval based on the total liquid water mixing ratio (droplets + raindrops) divided by the total condensate mixing ratio. The different line styles denote different CCN concentrations and different colors denote different INP concentrations.

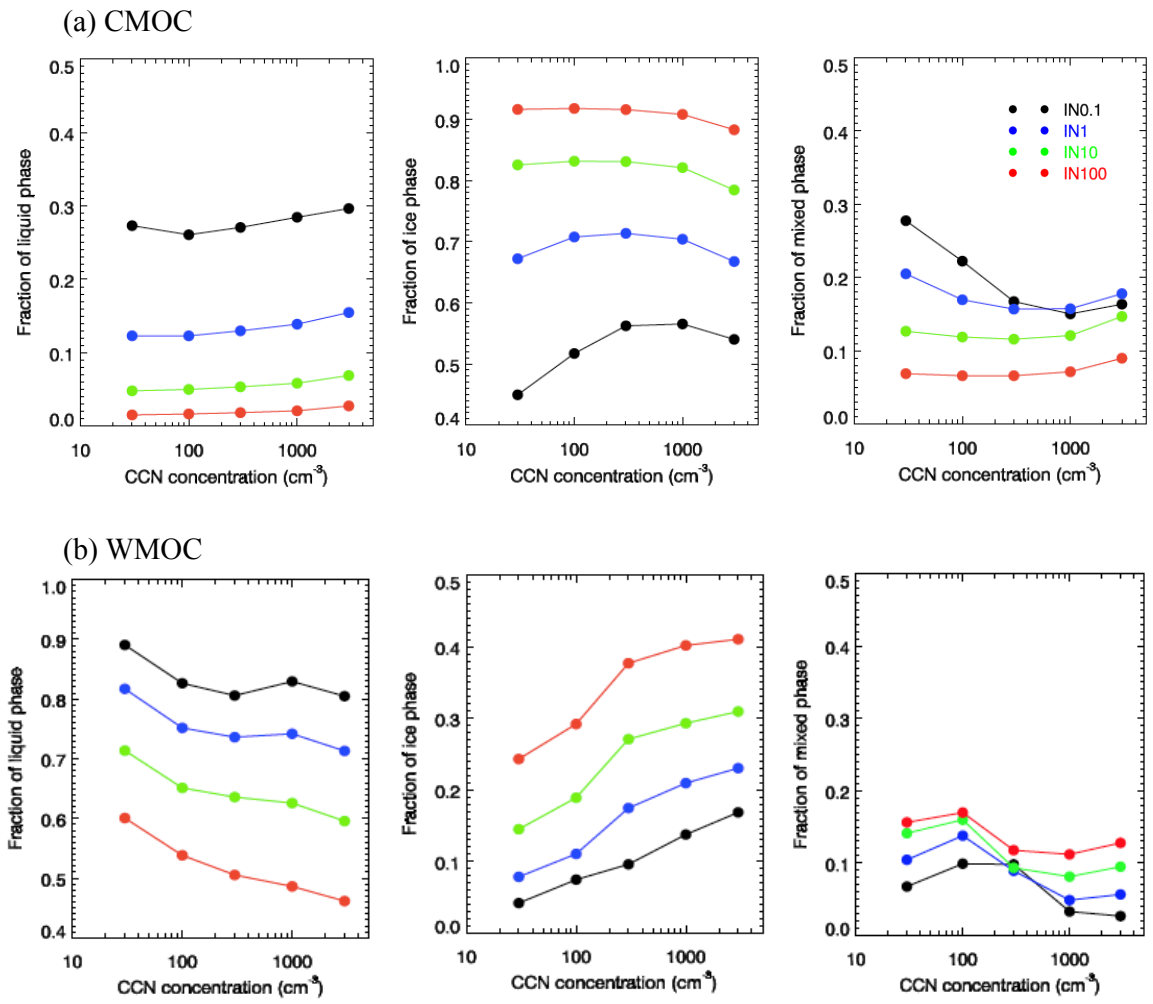

Fig. 13 The fraction of the liquid phase (left), ice phase (middle), and mixed-phase (right) for the (a) CMOC and (b) WMOC over the simulation period by excluding the initial two hours. The cloud phase for each cloud grid point that has a total condensate mass of larger than $1x10^{-5}$ kg kg^{-1} is identified based on the ratio of liquid to ice water mixing ratios. If the ratio is larger than 0.99 or smaller than 0.01, the grid point is identified as liquid phase or ice phase, respectively. Between these values is identified as mixed-phase. The fraction for each cloud phase is calculated by the number of grid points identified for the phase divided by the total number of the grid points of all three phases. So, the fractions of all three add up to 1 for each simulation case.

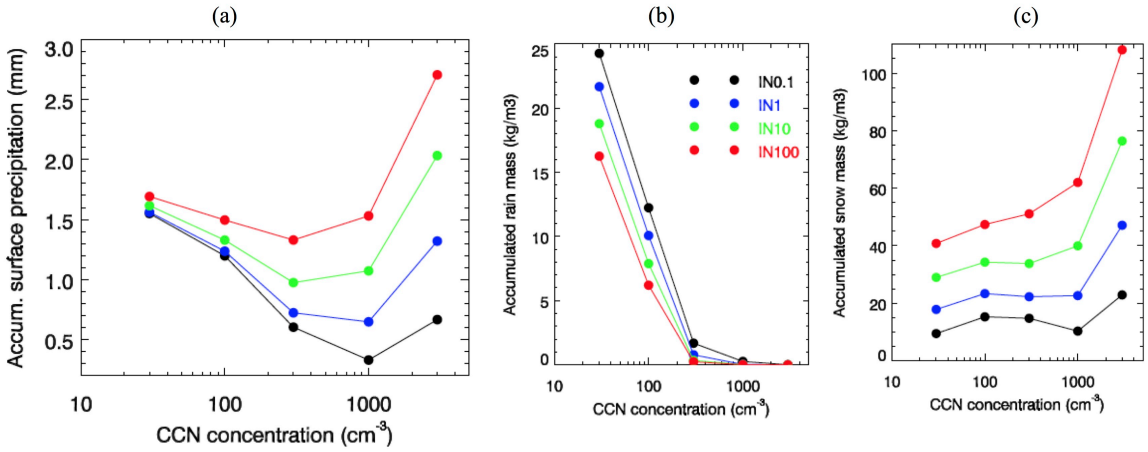

Fig. 14 Same as Fig. 2, except for the WMOC case.

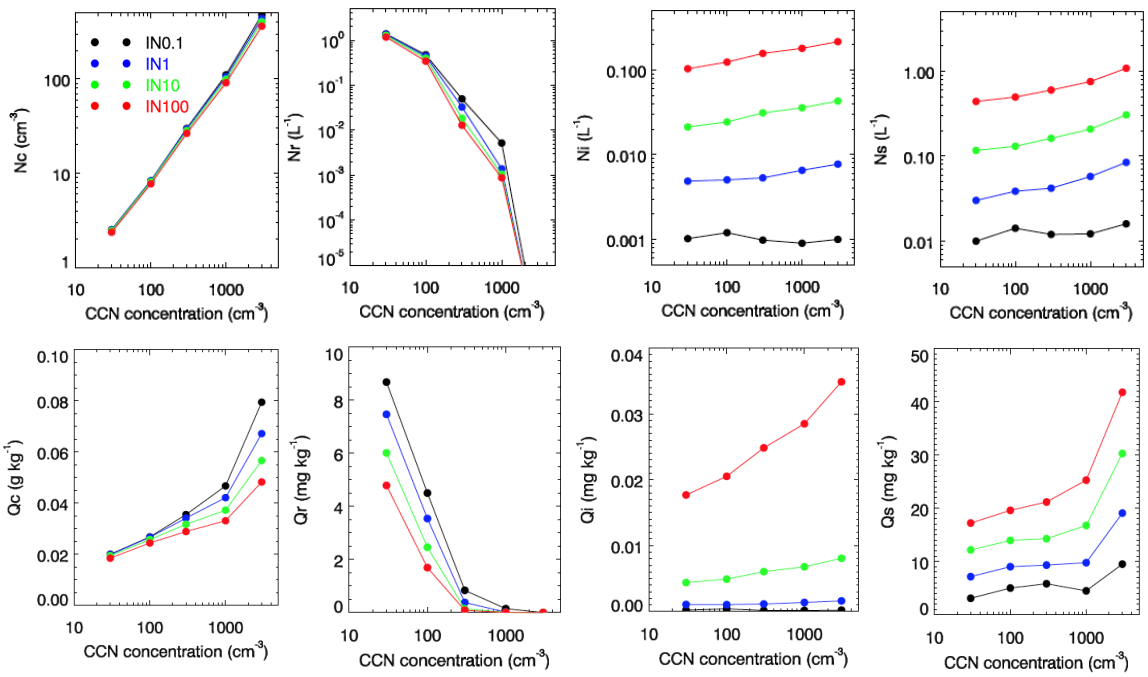

Fig. 15 Same as Fig. 3, except for the WMOC.

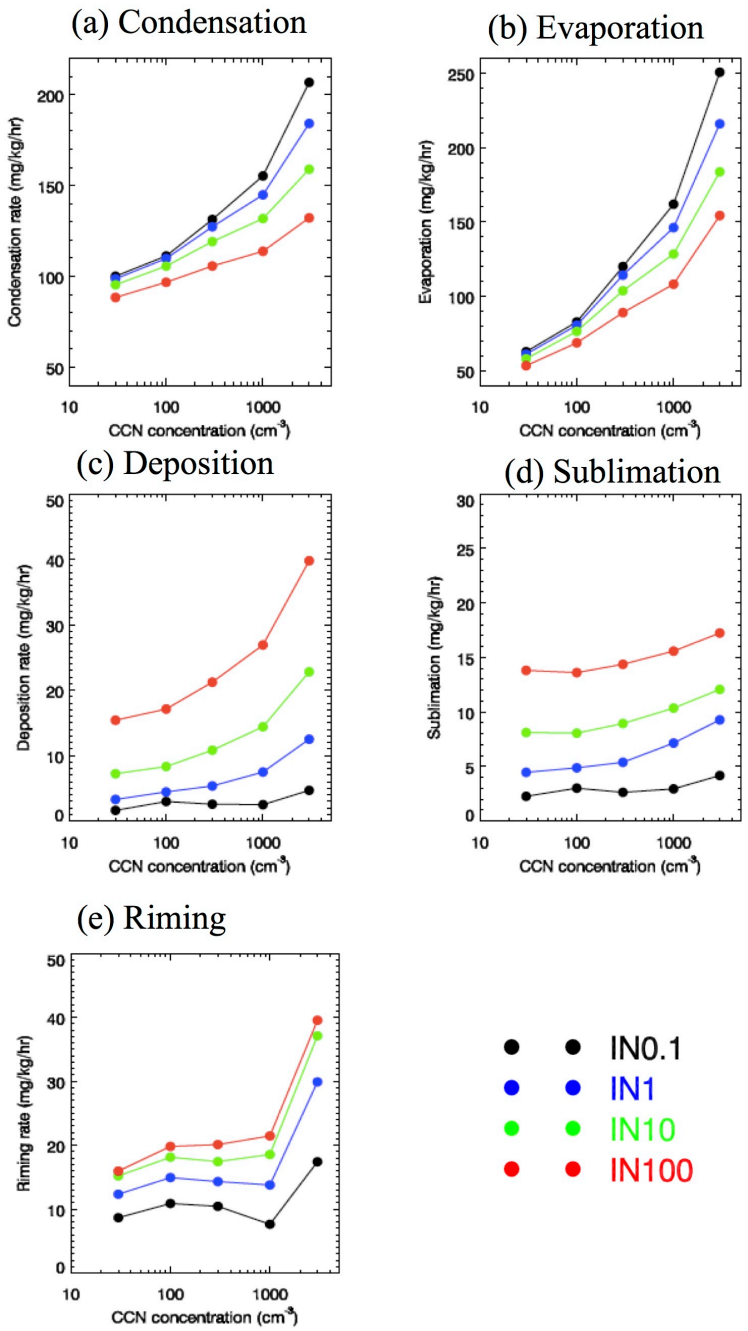

Fig. 16 Same as Fig. 4, except for the WMOC.

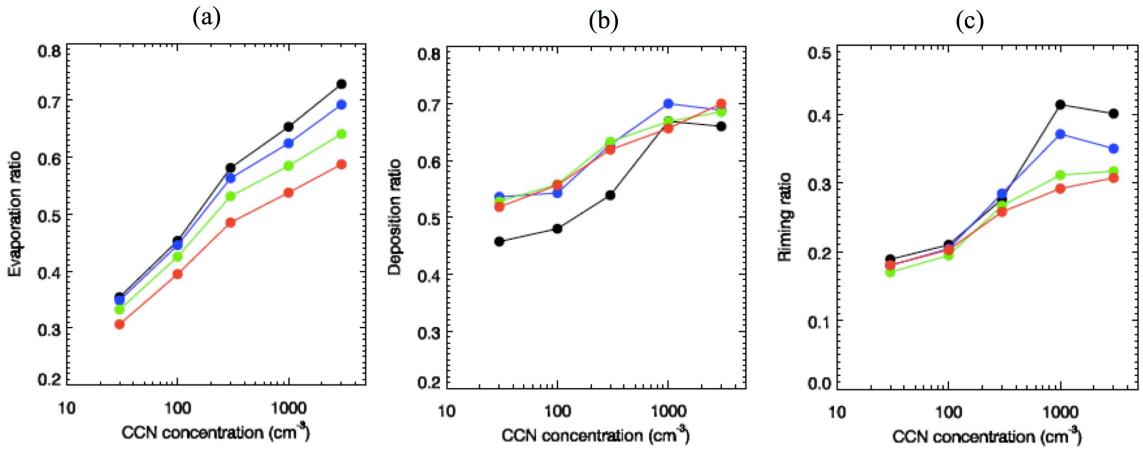

Fig. 17 Same as Fig. 5, except for the WMOC.